nature communications

Article

https://doi.org/10.1038/s41467-025-57414-4

Disruption of tryptophan metabolism by high-fat diet-triggered maternal immune activation promotes social behavioral deficits in male mice

Received: 4 January 2024

Accepted: 20 February 2025

Published online: 02 March 2025

Check for updates

Penghao Sun[1,6], Mengli Wang[1,6], Xuejun Chai[2] ✉, Yong-Xin Liu[3], Luqi Li[4], Wei Zheng[5], Shulin Chen[1], Xiaoyan Zhu[1] ✉ & Shanting Zhao[1] ✉

Diet-related maternal obesity has been implicated in neurodevelopmental disorders in progeny. Although the precise mechanisms and effective interventions remain uncertain, our research elucidates some of these complexities. We established that a prenatal high-fat diet triggered maternal immune activation (MIA), marked by elevated serum lipopolysaccharide levels and inflammatory-cytokine overproduction, which dysregulated the maternal tryptophan metabolism promoting the accumulation of neurotoxic kynurenine metabolites in the embryonic brain. Interventions aimed at mitigating MIA or blocking the kynurenine pathway effectively rescued the male mice social performance. Furthermore, excessive kynurenine metabolites initiated oxidative stress response causing neuronal migration deficits in the fetal neocortex, an effect that was mitigated by administering the glutathione synthesis precursor *N*-Acetylcysteine, underscoring the central role of maternal immune-metabolic homeostasis in male mice behavioral outcomes. Collectively, our study accentuated the profound influence of maternal diet-induced immuno-metabolic dysregulation on fetal brain development and provided the preventive strategies for addressing neurodevelopmental disorders.

Diet is a crucial factor in human health and plays a significant role in the prevalence of noncommunicable chronic diseases, now at epidemic levels[1]. Research in the United States indicates that over half of all females are either overweight or living with obesity at the time of pregnancy[2]. Excessive consumption of saturated fats is a primary factor contributing to this health concern[3]. Recent studies suggest that maternal obesity during pregnancy may elevate the risk of neurodevelopmental disorders, such as autism spectrum disorder (ASD) – characterized by repetitive behaviors and challenges in social interaction – in offspring[4,5]. Notably, neurodevelopmental disorders are two to four times more frequently diagnosed in males than in females[6]. Despite this, effective treatments for neurodevelopmental disorders remain limited[7]. Consequently, understanding how maternal diet impacts fetal development and health is imperative for devising

[1]College of Veterinary Medicine, Northwest A&F University, Yangling, Shaanxi, China. [2]College of Basic Medicine, Xi'an Medical University, Xi'an, Shaanxi, China. [3]Shenzhen Branch, Guangdong Laboratory of Lingnan Modern Agriculture, Genome Analysis Laboratory of the Ministry of Agriculture and Rural Affairs, Agricultural Genomics Institute at Shenzhen, Chinese Academy of Agricultural Sciences, Shenzhen, Guangdong, China. [4]Life Science Research Core Services, Northwest A&F University, Yangling, Shaanxi, China. [5]College of Resources and Environment Sciences, Northwest A&F University, Yangling, Shaanxi, China. [6]These authors contributed equally: Penghao Sun, Mengli Wang. ✉e-mail: xchai@xiyi.edu.cn; xyzhu0922@nwsuaf.edu.cn; zhaoshanting@nwsuaf.edu.cn

preventive strategies and therapies for neurodevelopmental disorders resulting from maternal HFD in the progeny.

Escalating evidence suggests an essential mechanism by which a high-fat diet (HFD) influences physiology and health is via the induction of a state of chronic metabolic inflammation, termed metaflammation[8]. Maternal health during pregnancy significantly influences the health and disease risk of offspring[9]. Rodent model studies show that a gestational HFD intensifies the production of inflammatory cytokines such as IL-1β, IL-6, and TNF-α in the plasma, liver, and brain tissue of both the mother and the fetus[10,11]. The maternal immune activation (MIA) hypothesis posits that inflammatory disturbances during gestation can influence fetal neurodevelopment[12–14], and human epidemiological studies substantiate a correlation between maternal inflammation during pregnancy and the incidence of neurodevelopmental disorders in offspring[15]. Meanwhile, MIA-induced behavioral changes in offspring exhibit a strong male bias[16]. Research in animals in which the innate immune system is engaged in directing brain masculinization has proposed the hypothesis that the male brain experiences a more inflammatory environment than the female brain during development, leading to male susceptibility to MIA[17]. However, little is known about whether maternal dietary-immune interactions are involved in disrupting fetal brain development and postnatal offspring behavioral phenotypes. Furthermore, as each proinflammatory state may involve multiple mechanisms[18], more rigorous evidence is required to ascertain the mechanisms linking diet-induced MIA with heightened susceptibility to neurodevelopmental disorders in male offspring.

Presently, it is widely acknowledged that tissue-specific and systemic immune responses and metabolic regulation are intricately connected, with one's proper function dependent on the other[19]. Disturbing this immune-metabolic homeostasis can lead to various chronic metabolic disorders, particularly neurodevelopmental and autoimmune diseases[20]. Our recent study indicates that a sustained HFD triggers an inflammatory response mediated by gut microbes, which disrupts peripheral tryptophan (Trp)-kynurenine (Kyn) metabolism[21]. Various pathologies of the central nervous system (CNS) are accompanied by dysfunction in Trp metabolism[22]. The Kyn pathway, tightly controlled by the immune system, serves as the prime metabolic route for Trp degradation[23]. The dysregulation of this pathway often results in excess production of neuroactive metabolites that regulate glutamate receptor-mediated neurotoxicity and free radical production[24]. This phenomenon is implicated in neurodevelopmental and psychiatric disorders[24,25]. However, whether disrupted interactions between maternal immune activities and metabolic responses help create a mechanistic understanding of maternal HFD-induced behavioral deficiencies in male offspring remains the subject of study.

Here we report that prenatal HFD induced inflammatory response in mice during pregnancy that precipitated behavioral impairments in male offspring, a condition ameliorated by the administration of (+)-Naloxone, a toll-like receptor 4 (TLR4) antagonist. Furthermore, maternal HFD-induced MIA upregulated the Trp-Kyn pathway in both maternal circulation and fetal forebrain, causing the accumulation of neuroexcitatory Kyn metabolites in the embryonic brain. Administrating HFD-fed mice with 1-methyltryptophan (1MT) effectively inhibited the Kyn pathway to rescue social behavioral deficits of male offspring, reinforcing the central role of the deregulated Kyn pathway in maternal HFD-induced male offspring behavioral deficits. The built-up Kyn metabolites initiated the oxidative stress response and lipid peroxidation in the fetal brain, causing neuronal migration deficits in the cerebral cortex. Supplementing HFD-fed mice with *N*-Acetylcysteine (NAC), a precursor for glutathione synthesis, further confirmed these observations during gestation. Collectively, our results provide the mechanistic insight into maternal HFD-associated social behavioral deficits in male offspring as a consequence of up-regulated MIA interfering with the Kyn pathway to cause neurodevelopmental abnormalities in the fetal brain.

Results

Differential impact of prenatal and postnatal maternal HFD on male offspring social behavior

Current epidemiological research suggests a link between maternal HFD and the onset of neurodevelopmental disorders[26]. Diverse prenatal and postnatal factors can modulate offspring susceptibility to such disorders in myriad ways[12]. To disentangle the effects of maternal pre-pregnancy and postnatal HFD on offspring behavioral outcomes, cross-fostering experiments were conducted, involving the exchange of newborns between mothers on a standard diet and those on HFD (Fig. 1a)[27]. At six weeks of age, female mice were assigned to either a control diet or HFD for 6 weeks, before being paired with males to reproduce. The resulting offspring were then switched at birth to new mothers, with litters between 1 and 5 days old (which were removed) (Fig. 1a). Persistent HFD resulted in a significant increase in maternal weight (Fig. S1a) and a reduction in litter size (Fig. S1b). Despite these maternal effects, no significant difference in body weight was observed between male offspring from mothers on a control diet (mCD) and those exposed to prenatal HFD (mHFD) at postnatal day 35 (P35, Fig. S1c), when behavioral tests were conducted (Fig. 1a). Notably, pups fostered by mothers on the HFD (mC-H) exhibited higher weight gain (Fig. S1c). We evaluated social behavior, including sociability and social preference, using an adaptation of the three-chamber social interaction paradigm (Fig. 1b). In testing sociability, we measured the time in which the subject mice interacted with either a stranger mouse (Mouse 1) or an empty wired cup (Empty, Fig. 1b). Male offspring from mHFD (oHFD) displayed compromised sociability, as reflected by no preference for stranger mice over empty cups (Fig. 1c). Alternatively, in comparison to oCD male offspring, a reduced interaction time with a mouse was evident in oC-H male offspring (Fig. S1d), although they demonstrated significant sociability (Fig. 1c). Social preference was determined by comparing the time spent by mice interacting with a familiar (Mouse 1) versus a stranger mouse (Mouse 2). Both oCD and oC-H male offspring spent significantly more time interacting with a new mouse than a familiar one, indicating normal novelty preference (Figs. 1d, S1e). In contrast, oHFD male offspring did not prefer interaction with stranger mice (Figs. 1d, S1e). Additionally, sustained maternal HFD both pre-pregnancy and post-partum led to increased marble-burying behavior in male offspring, indicating an enhanced inclination towards restrictive and repetitive activities (Fig. 1e). This behavioral deficit was found to be particularly pronounced in oHFD male offspring as compared to oC-H male offspring (Fig. 1e). In conclusion, our results suggest that continuous maternal HFD, particularly during the prenatal stage, significantly impaired the social behavior in male offspring.

Maternal HFD induces immune activation resulting in male offspring behavioral deficits

Nutrient and resource absorption by the developing fetus is solely reliant on maternal circulation, underlining the importance of maternal health during pregnancy in influencing offspring development[28]. To uncover the effects of dietary insults on systemic homeostasis in pregnant mice, we assessed concentrations of 92 proteins in sera of the gestational day (GD) 18.5 mice employing the Olink Proteomics method. Principal component analysis (PCA) of these proteins revealed a distinct separation between mCD and mHFD mice ($p < 0.001$, Fig. 2a). Differentially expressed proteins (DEPs) analysis revealed 58 proteins significantly disturbed by maternal diet ($p < 0.05$, Fig. 2b). Pathway enrichment analysis based on DEPs informed that prenatal HFD triggered maternal immune activation (MIA) (Figs. 2c, S2a). Notably, the interleukin-17 (IL-17) pathway was significantly upregulated in mHFD mice (Fig. 2c), as evidenced by enhanced

https://doi.org/10.1038/s41467-025-57414-4

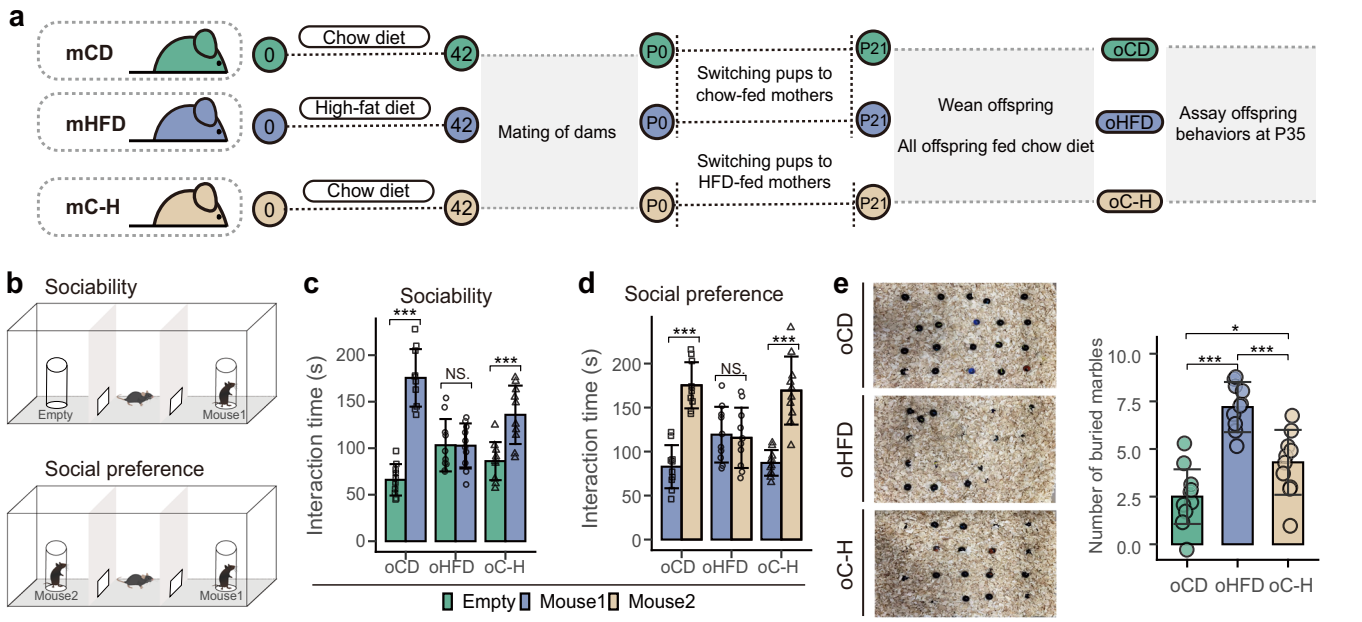

Fig. 1 | Maternal high-fat diet impairs male offspring behavioral outcomes. **a** Schematic of the maternal diet regimen and breeding. **b** Schematic of the three-chamber social interaction task. **c** In the sociability test, oCD and oC-H male offspring spent more time interacting with a mouse than with an empty wire cage, whereas oHFD male offspring showed no preference for the mouse ($n = 10$ mice, 10 litters/group; oCD: $t = 9.835$, $p = 1.195e\text{-}07$; oHFD: $t = 0.43$, $p = 0.966$; oC-H: $t = 4.202$, $p = 0.0007226$). **d** In the social novelty test, unlike oCD and oC-H, oHFD male offspring exhibited no preference for interacting with a novel versus a familiar mouse ($n = 10$ mice, 10 litters/group; oCD: $t = 8.153$, $p = 1.931e\text{-}07$; oHFD: $t = 0.244$, $p = 0.810$; oC-H: $t = 6.290$, $p = 4.835e\text{-}05$). **e** Images (left) and quantification (right) of the number of buried marbles ($n = 10$ mice, 10 litters/group; $F_{2,27} = 9.434$, oCD vs oHFD: $p = 4.3e\text{-}07$, oHFD vs oC-H: $p = 0.00053$, oCD vs oC-H: $p = 0.036$). Data are represented as mean ± SD. In **c** and **d** p-values were determined by the two-sided unpaired Student's t-test. In **e** statistical significance was assessed by one-way analysis of variance (ANOVA) with Bonferroni's multiple comparison test. Source data are provided as a Source Data file. NS not significant, *p-value ≤ 0.05, **p-value ≤ 0.01, ***p-value ≤ 0.001.

expression of IL17a and IL17f (Figs. 2b, Fig. S2c), which has been shown to promote neurodevelopmental disorders in offspring[29]. Activation of the IL-17 signaling pathway is commonly recognized as a response to infectious agents (e.g. *Escherichia coli*)[30]. We confirmed, in recent studies, that sustained HFD encourages the proliferation of lipopolysaccharide (LPS)-producing bacteria, thus increasing circulating endotoxin concentrations, subsequently evoking TLR4-mediated systemic inflammatory response[21,31]. Similarly, prenatal HFD increased serum LPS levels in pregnant mice (Fig. 2d) and enhanced the LPS-mediated signaling pathway and toll-like receptor signaling pathway (Figs. 2c, S2a).

Chronic inflammation during pregnancy has been associated with the onset of neurodevelopmental and psychiatric complications in offspring[12]. To determine the role of MIA in HFD-induced offspring behavioral deficits, (+)-Naloxone, an antagonist of TLR4[32], was administered to HFD-fed mice during pregnancy (mH-Nalo, Fig. 2e). mH-Nalo mice, compared to mCD mice, exhibited prominently different serum protein profiles at GD 18.5 ($p = 0.0027$, Fig. 2a). Essential observation was the ability of prenatal (+)-Naloxone to inhibit HFD-induced MIA, downregulate the IL-17 signaling pathway, and suppress the expression of proinflammatory cytokines IL-17a and IL-17f (Figs. 2f–g, S2b). The inhibitory effect of (+)-Naloxone on HFD-induced maternal immune responses was confirmed by ELISA assay results (Fig. S2c). This effect safeguarded the social behavior traits in the three-chamber test for oH-Nalo male offspring (Fig. 2h). Moreover, oH-Nalo male offspring illustrated lower levels of stereotyped marble-burying behavior (Fig. 2i). To further explore the role of upregulated IL-17 expression in maternal HFD-induced social behavior deficits in offspring, pregnant mice were systemically administered an IL-17a antibody (mH-Anti-IL17a) to block IL-17 signaling or an IgG1 isotype as a control (mH-IgG1) beginning at GD0.5 (100 μg/mouse/2 days, Fig. 2j). Compared to the IgG1 injection, the IL-17a-blocking antibody administration effectively rescued social behavioral deficits in the offspring (Fig. 2k–l). These findings propose the maternal HFD-induced MIA as a key player in modulating male offspring behavioral deficits.

Association between MIA and upregulation of the maternal Kyn pathway

While MIA has been previously identified as a critical factor affecting the disease-related phenotypes of the offspring[33], there is still limited understanding of how MIA contributes to brain development. Empirical studies provide convincing evidence of obesity and dietary factors, despite their proinflammatory nature, on neurodevelopment through metabolic stress, oxidative stress, and neuroendocrine mechanisms[34]. To uncover the response of serum metabolites to the maternal diet, we conducted untargeted metabolomics on the serum of mice at gestational day 18.5 (GD18.5). PCA results demonstrated a significant variation in serum metabolic profiles between mice scores in the mCD group and those in the mHFD group along dimension 2 (Fig. 3a). The variation in serum metabolites was found to be mitigated by (+)-Naloxone administration (Fig. 3a), alluding to a potential association between diet-induced MIA and maternal metabolic transitions. Co-expression analysis is a common tool to investigate molecular pathways that underlie disease phenotypes[35]. To elaborate on the metabolic response connected with maternal HFD-induced immune response, a weighted correlation network analysis (WGCNA) was performed on the 8950 serum metabolites from the 18 samples ($n = 6$ for mCD, mHFD, and mH-Nalo). This analysis clustered the serum metabolites into 16 co-expression modules, each normatively designated by a specific color (Fig. 3b). Subsequent analyzes of these modules were used to estimate eigenmetabolite, as a summary metric signifying the aggregate metabolite expression of each module. Correlation analysis between eigenmetabolite and serum

https://doi.org/10.1038/s41467-025-57414-4

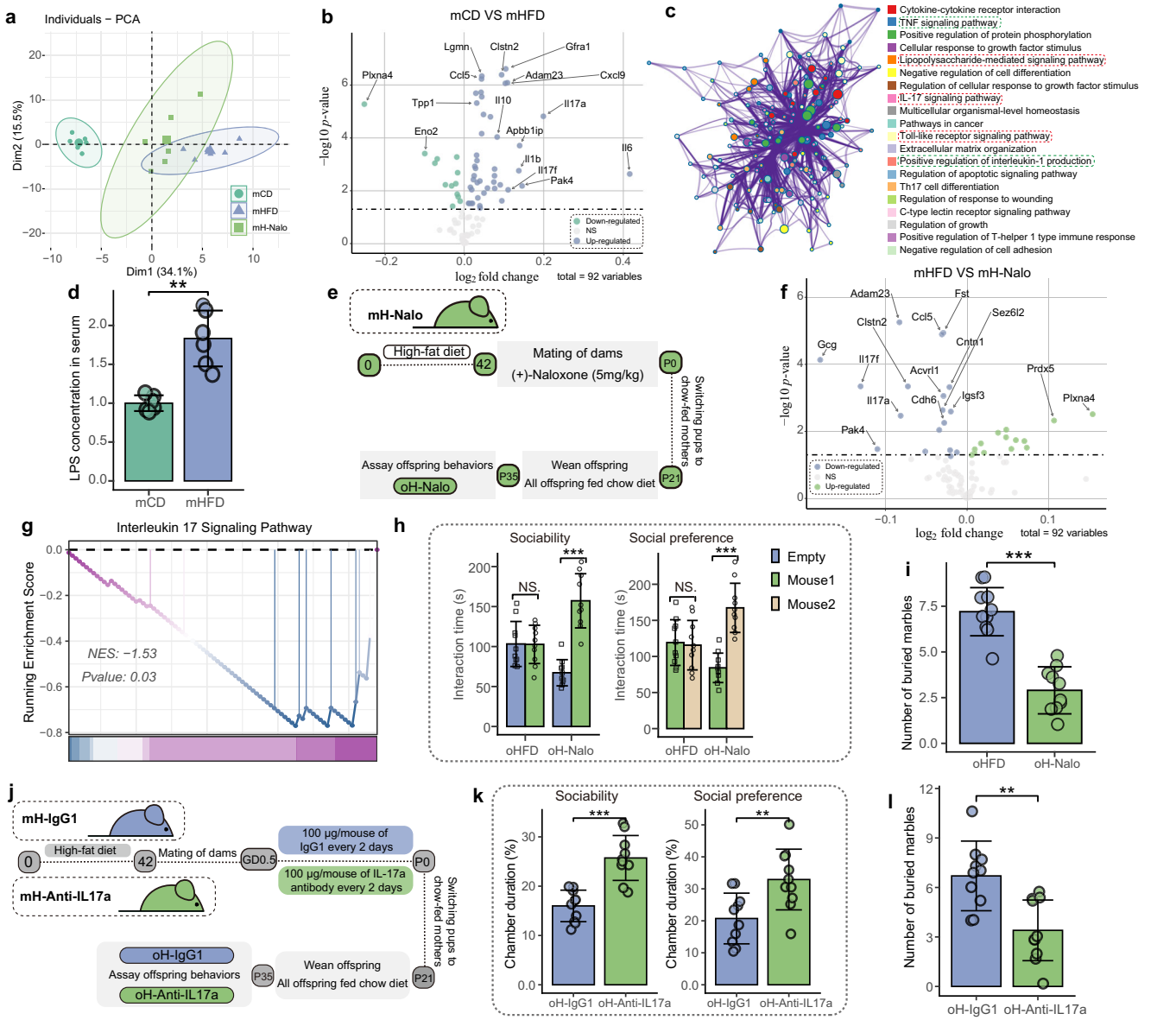

Fig. 2 | HFD triggers maternal inflammation linked to behavioral deficits in male offspring. a PCA score plot of serum proteomic data ($n = 6$ mice/group). **b** Volcano plots showing serum protein changes in HFD versus normal diet-fed mice at GD18.5. **c** Metascape enrichment network for HFD-altered serum protein ($p < 0.05$). **d** HFD increased lipopolysaccharide in maternal serum (normalized to mCD; $n = 6$ mice/group; $t = 5.462$, $p = 0.002$). **e** Schematic of (+)-Naloxone administration (mH-Nalo). **f** Volcano plot of (+)-Naloxone-altered serum proteins in HFD-fed mice. **g** (+)-Naloxone inhibited IL-17 signaling pathway. **h** (+)-Naloxone rescued social behavior deficits in male mice ($n = 10$ mice, 10 litters/group; sociability: oHFD: $t = 0.43$, $p = 0.966$; oH-Nalo: $t = 7.562$, $p = 4.143e\text{-}06$; social preference: oHFD: $t = 0.244$, $p = 0.810$; oH-Nalo: $t = 6.620$, $p = 8.988e\text{-}06$). **i** (+)-Naloxone reduced marble-burying number ($n = 10$ mice, 10 litters/group; $t = 7.387$, $p = 7.513e\text{-}07$). **j** IL-17 cytokine blockade experimental design. IL-17A blocking antibody rescued the social performance (**k,** $n = 10$ mice, 10 litters/group; sociability: $t = 5.53$, $p = 4.43e\text{-}05$; social preference: $t = 3.116$, $p = 0.006$; **l,** $n = 10$ mice, 10 litters/group; $t = 3.729$, $p = 0.002$). Data are represented as mean ± SD. In **a**, permutational multivariate analysis of variance (PERMANOVA) by Adonis was used to determine statistical significance ($F = 3.885$, $p = 8.412e\text{-}06$). In **b** and **f** statistical significance was assessed by a two-sided unpaired t-test, adjusted using the false discovery rate (FDR) method. In **g** the enrichment score was calculated, normalized to obtain the Normalized Enrichment Score (NES). Nominal *P*-values were computed using an empirical phenotype-based permutation test (999 permutations), with multiple comparisons corrected by FDR. In **d**, **h**, **i**, and **k**–**l** *p*-values were determined by the two-sided unpaired Student's t-test. Source data are provided as a Source Data file. LPS Lipopolysaccharide.

proteins, impacted by maternal diet ($n = 58$), demonstrated that the MEorange and MEblack modules were positively co-varied with the serum levels of proinflammatory cytokines such as IL1b, IL6, Tnfrsf11b, IL17a, and IL17f (Fig. 3c). Notably, (+)-Naloxone administration effectively reversed the maternal HFD-influenced patterns of eigenmetabolite in the MEblack module but not in the MEorange module (Fig. 3d), suggesting that the metabolites in the MEblack module were more susceptible to inflammation related to maternal HFD.

To extract more insight into MIA-induced metabolic stress, quantitative metabolite sets enrichment analysis (qMSEA) was performed on the metabolites of the MEblack module, leading to the revelation that pathways relating to Trp metabolism and glutathione metabolism were significantly overrepresented (Fig. 3e). Our previous study exhibited a strong association between disrupted Trp metabolism and neurological disorders in mice with obesity[31]. Consequently, this work further scrutinized the levels of Trp metabolites in the maternal serum and found an evident upregulation of the Kyn pathway

https://doi.org/10.1038/s41467-025-57414-4

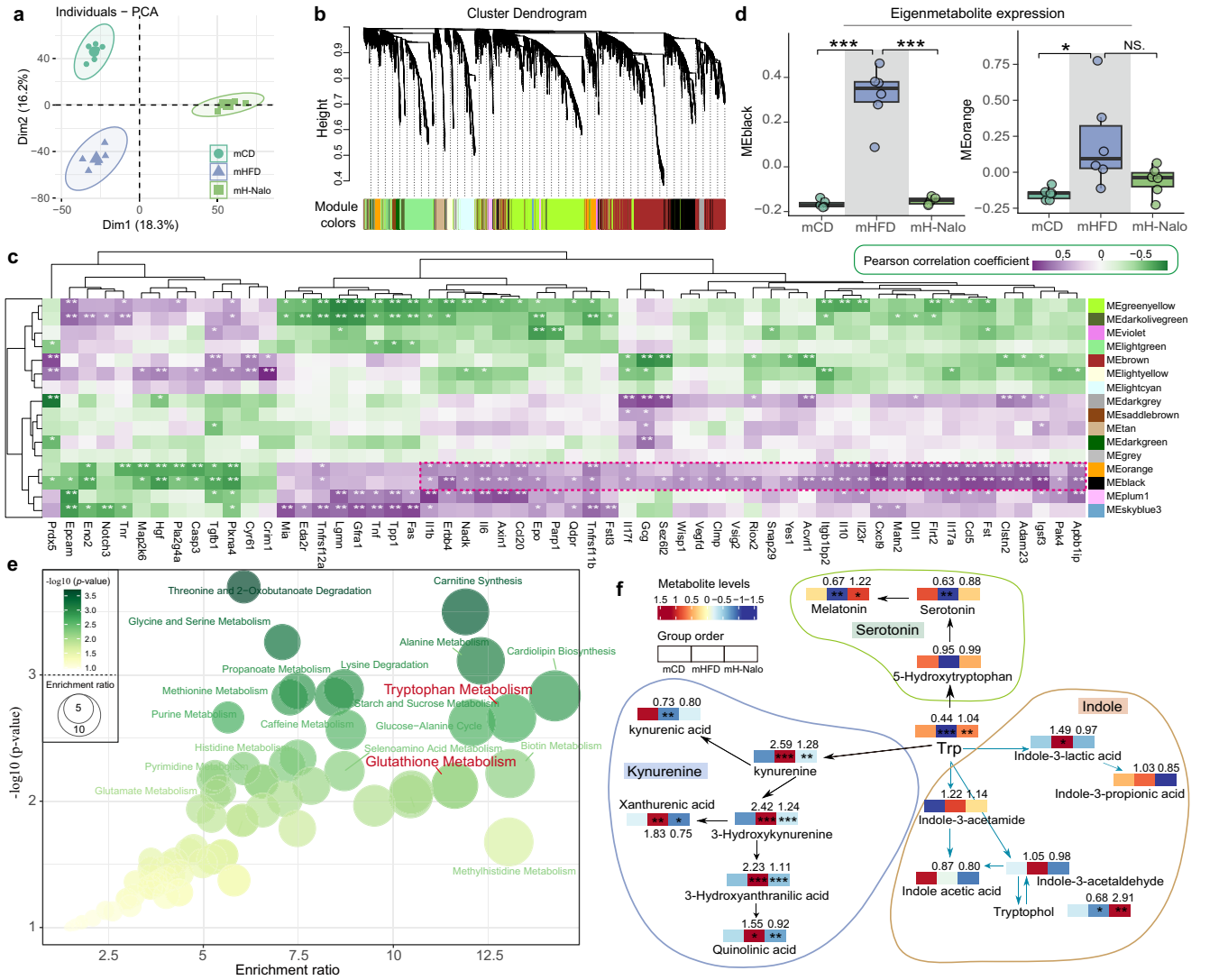

Fig. 3 | HFD-induced MIA promotes the kynurenine pathway in maternal circulation. a PCA of serum metabolic profiles ($n = 6$ mice/group). **b** WGCNA cluster dendrogram grouped serum metabolites into modules M1-16. **c** Correlation heatmap between metabolite modules and HFD-altered serum proteins. **d** Module eigengene expression across groups ($n = 6$ mice/group; MEblack: $F_{2,15} = 79.902$, mCD vs mHFD: $p = 2.41e\text{-}08$, mHFD vs mH-Nalo: $p = 3.62e\text{-}08$; MEorange: $F_{2,15} = 5.429$, mCD vs mHFD: $p = 0.012$, mHFD vs mH-Nalo: $p = 0.058$). **e** qMSEA identified metabolic pathways of MEblack module. **f** Summary of perturbed tryptophan metabolism pathways in serum ($n = 6$ mice/group; mCD vs mHFD: Trp, $t = 5.002$, $p = 0.0002847077$; Kyn, $t = 5.569$, $p = 0.0001679119$; 3-HK, $t = 5.004$, $p = 0.0003999991$; Kyna, $t = 3.884$, $p = 0.003$; Quin, $t = 2.594$, $p = 0.03$; Xanthurenic Acid, $t = 2.994$, $p = 0.01$; 3-HAA, $t = 6.103$, $p = 7.704395e\text{-}05$; Serotonin, $t = 4.228$, $p = 0.002$; Melatonin, $t = 3.216$, $p = 0.009$; ILA, $t = 2.591$, $p = 0.03$; Tryptophol, $t = 2.611$, $p = 0.03$; mHFD vs mH-Nalo: Trp, $t = 4.511$, $p = 0.001$; Kyn, $t = 4.383$, $p = 0.001$; 3-HK, $t = 4.994$, $p = 0.0004063576$; Quin, $t = 4.517$, $p = 0.001$; Xanthurenic Acid, $t = 3.629$, $p = 0.005$; 3-HAA, $t = 4.738$, $p = 0.0006114107$; Melatonin, $t = 2.443$, $p = 0.03$; Tryptophol, $t = 4.005$, $p = 0.002$). In **d** data are represented as mean ± SD. In **a** Adonis was used to determine statistical significance ($F = 7.704$, $p = 5.374e\text{-}07$). In **c** statistical significance was determined using a two-tailed unpaired Student's t-test, with multiple comparisons corrected using the FDR method. Statistical significance in (**d**) was determined using a ANOVA followed by Dunnett's multiple comparison test, and in (**f**) a two-tailed unpaired Student's t-test was used. In **e** p-value was determined using permutation testing (999 permutations) with adjustment using FDR. Enrichment ratio = Hits / Expected. Source data are provided as a Source Data file.

in mHFD mice, as marked by depleted Trp reserves (0.44-fold) and increased levels of Kyn (2.59-fold), 3-hydroxykynurenine (3-HK, 2.42-fold), 3-hydroxyanthranilic acid (3-HAA, 2.23-fold), xanthurenic acid (1.83-fold), and quinolinic acid (Quin, 1.55-fold) (Fig. 3f). Notably, (+)-Naloxone administration significantly reduced maternal serum levels of Kyn metabolites, while exerting minimal effects on serotonin and other metabolites in the indole pathway (Fig. 3f). Concomitantly, consistent with the beneficial effects on offspring social behavioral phenotypes, blockade of the IL-17 pathway effectively inhibited the accumulation of Kyn and 3-HK in maternal serum (Fig. S3f). These findings suggest that the HFD-induced maternal immune response, particularly the activation of the IL-17 pathway, predominantly triggered the Kyn pathway of Trp metabolism in the maternal circulation.

Maternal HFD-induced MIA promotes the Kyn-Quin pathway in the fetal forebrain

Kyn and its associated metabolites, cumulatively termed "kynurenines," are renowned for their effects on the CNS and have been implicated in numerous mental and psychiatric disorders[36]. Like Trp, Kyn and 3HK readily cross the blood–brain barrier[37]. A distinctive metabolic pattern (Fig. S3a) coupled with elevated levels of Kyn and 3HK (Fig. S3b), consistent with findings in the maternal serum (Fig. S3c–e), was observed in the mHFD fetal forebrain at embryonic day 18.5 (E18.5). Microglia, the resident innate immune cells in the CNS, control the Kyn-Quin metabolism(Fig. 4a)[38]. We noticed that microglia (Iba1-positive cells) were primarily located in the ventricular zone (VZ) of the E18.5 fetal neocortex (Fig. 4b). Consistent with the enhanced

https://doi.org/10.1038/s41467-025-57414-4

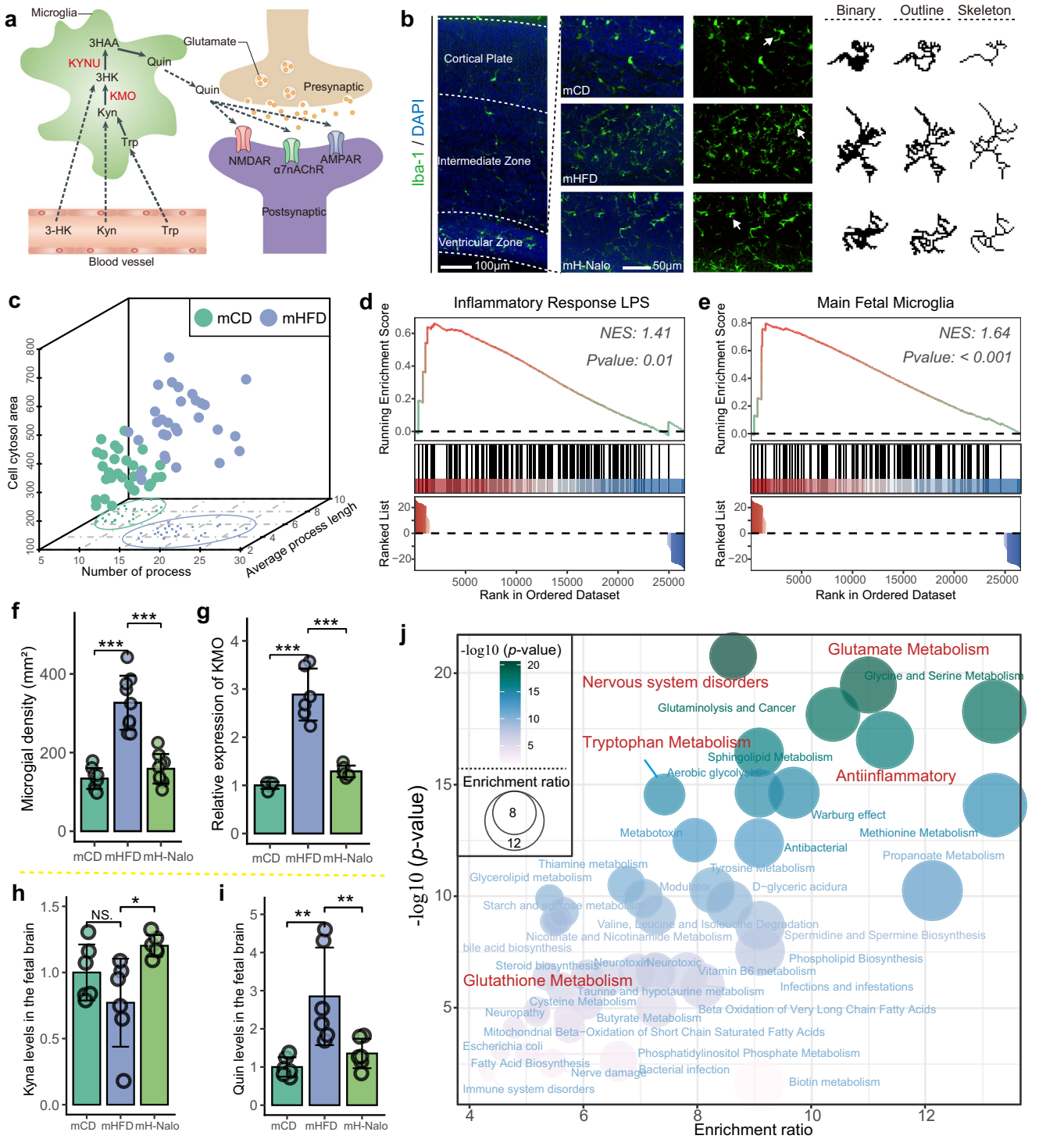

Fig. 4 | Maternal HFD enhances Quin production in the fetal forebrain. a Kyn metabolism in microglia. **b** Confocal images and skeleton analysis of microglia labeled with Iba-1 in fetal brain. **c** Microglia morphologies in mCD and mHFD fetal brain ($n = 30$ cells from 3 mice). GSEA showing enrichment of the inflammatory response LPS pathway (**d**) and main fetal microglia pathway (**e**) ($n = 3$ for each group). (+)-Naloxone administration decreased the microglial density (**f**) $n = 9$ slices from 3 mice, 3 litters/group; $F_{2,24} = 43.474$, mCD vs mHFD: $p = 1.80e\text{-}08$, mHFD vs mH-Nalo: $p = 2.08e\text{-}07$) and mRNA expression of Kynurenine-3-monooxidase (KMO) (**g**) $n = 6$ mice, 6 litters/group; $F_{2,15} = 59.674$, mCD vs mHFD: $p = 8.09e\text{-}08$, mHFD vs mH-Nalo: $p = 6.98e\text{-}07$) in the fetal brain. The concentrations of Kyn (**h**) $F_{2,15} = 5.516$, mCD vs mHFD: $p = 0.187$, mHFD vs mH-Nalo: $p = 0.011$) and Quin (**i**) $F_{2,15} = 9.394$, mCD vs mHFD: $p = 0.002$, mHFD vs mH-Nalo: $p = 0.009$) in the fetal brain tissue among three groups ($n = 6$ mice, 6 litters/group). **j** qMSEA identified the metabolic pathways in the fetal brain significantly perturbed by maternal HFD ($p < 0.05$). Data are represented as mean ± SD. In **d**,**e** NES was calculated as described above. Statistical significance was determined using permutation testing (999 permutations), with FDR correction. In **g**–**i** data are normalized to mCD. In **f**–**i** p-values were determined by ANOVA with Dunnett's multiple comparison test. In **j**, enrichment ratio was calculated as described above, and statistical significance was assessed through permutation testing (999 permutations) with FDR correction. Source data are provided as a Source Data file. KYNU Kynureninase, KMO Kynurenine 3-monooxygenase, Iba-1 Ionized calcium binding adapter molecule 1, DAPI 4′,6-Diamidino-2-phenylindole, NMDAR N-methyl-D-aspartic acid receptor, α7nAChR α7 nicotinic acetylcholine receptor, AMPAR α-Amino-3-hydroxy-5-methyl-4-isoxazole propionic acid receptor.

maternal inflammatory responses (Fig. 2b–d), gene set enrichment analysis (GSEA) based on RNA-seq data indicated significant upregulation of the "inflammatory response LPS" pathway in mHFD fetal brain at E18.5 (Fig. 4d). Extant studies have highlighted that LPS exposure accelerates microglia development in mice (Fig. 4e)[39]. As microglia function in response to environmental cues, alterations in microglia morphology can point to changes in CNS immune activities and potential dysfunction[40]. Examining the density and morphological features of microglia, we found an uptick in microglia density (Fig. 4f) and complexity of traits, such as cellular cytosol area, process number, and average process length (Figs. 4c, S4a), in mHFD fetal brain, indicating an increased inflammatory response. Besides, there was a significant rise in the kynurenine 3-monooxygenase (KMO) mRNA expression in the mHFD fetal brain (Fig. 4g), driving the transformation of Kyn to neuroactive and neurotoxic metabolites (Fig. 4a)[41]. This metabolic shift was further validated by the upregulation of the "Trp metabolic process" pathway, characterized by higher kynureninase (KYNU) mRNA expression, in the mHFD fetal brain (Fig. S4c). Furthermore, metabolomics analysis distinguished 1932 significantly modified metabolites between mCD and mHFD E18.5 fetal forebrain ($p < 0.05$), interplay with Trp metabolism and anti-inflammatory pathway (Fig. 4j). Consequently, Quin level in the fetal brain of mHFD mice was substantially higher compared to that of control diet mice (Fig. 4i).

The Kyn pathway is known to be activated by proinflammatory cytokines and TLR ligands[42]. Interestingly, (+)-Naloxone administration in HFD-fed mice during pregnancy inhibited the peripheral Trp-Kyn pathway (Fig. 3f). Concurrently, the hyperactivity of microglia in the fetal forebrain of mH-Nalo was mitigated (Fig. S4d), resulting in decreased microglia complexity and density (Figs. 4b, 4f, S4a). The transcriptional profile of the mH-Nalo fetal brain was analogous to that of control diet mice (Fig. S4b), indicating that MIA predominantly determined the maternal HFD-triggered disruption in fetal brain development. Furthermore, with (+)-Naloxone administration, the decrease in KMO and KYNU mRNA expressions (Figs. 4g, S4d) led to the restraining of the Trp metabolism pathway (Fig. S4d), which subsequently inhibited the production of Kyn metabolites (e.g. 3HK and Quin) in the fetal forebrain (Figs. S3b, 4i). Similarly, inhibition of the Trp-Kyn metabolic shift in the embryonic brain was observed in mH-Anti-IL17 (Fig. S3g). Lastly, the enhancement in kynurenic acid (Kyna) concentration in mH-Nalo fetal forebrain was noticed (Fig. 4h), a compound linked with neuronal protection[43]. In summary, our findings suggest a predominant role of maternal diet-induced immune activation in Kyn pathway activation and neurotoxic Quin accumulation in the fetal brain.

Maternal Trp modulation affects behavioral outcomes in the male offspring of HFD-fed mice

It was observed that maternal HFD-induced MIA brought about Trp metabolism dysfunction. Hence, we sought to understand if this metabolic response contributed to social behavioral deficits in progeny. Prior research indicated that serum Trp metabolites increase dose-dependently with dietary Trp intake[44]. Subsequently, Trp addition to the drinking water (0.8%)[45] of gestational mice on a control diet (mC-Trp) or HFD (mH-Trp) was carried out (Fig. 5a). As envisaged, this led to a boost in Trp level in maternal circulation and fetal forebrain (Fig. 5b). Interestingly, the oC-Trp male offspring showed no significant difference in their social performance when compared with oCD male offspring (Figs. 5c, S5a–c). On the other hand, extra Trp supplementation in HFD-fed mice led to enhancements in Kyn pathway metabolites, especially marked in Quin production within the fetal brain (Fig. 5b). Additionally, more severe stereotypic behavior was observed in the marble-burying test as per the oH-Trp male offspring, though the three-compartment test showed no difference when compared to oHFD male offspring, a potential floor effect due to low social performance (Figs. 5c, S5a–c). To reaffirm the influence of maternal Kyn metabolites concerning social behavioral deficits in offspring, gestational mice under HFD were treated with 1-methyltryptophan (1MT), an indoleamine-pyrrole 2,3-dioxygenase 1 (IDO1) antagonist to inhibit Kyn production (mH-1MT, Fig. 5a). By inhibiting the Kyn pathway (Fig. 5b), 1MT effectively counteracted maternal HFD-induced behavioral deficits, evident through reduced marble-burying and improved three-chamber test performance in the oH-1MT male offspring (Fig. 5c, S5a-c).

To unravel the mechanisms responsible for generating behavioral deficits in offspring as a result of maternal Kyn pathway dysfunction, the fuzzy C-means algorithm[46] was employed on RNA-seq data obtained from the E18.5 fetal forebrain (Fig. 5d). We recognized a total of ten distinct gene clusters that responded to various regulatory factors (Figs. S6, 5d). Notably, the relative expression of clusters 1 and 6 correlated significantly with Kyn concentration in the fetal forebrain (Fig. 5c). Pertinently, GSEA based on these two clusters revealed that the processes related to microtubule organization and movement, crucial for neuronal migration, were down-regulated, indicating compromised development and localization of neurons in mHFD fetal forebrain (Figs. S7a, b). Thus, these findings suggest that the dysregulated Kyn pathway in the fetal brain may detrimentally affect the male offspring social behavior by impacting the migration and localization of newborn neurons.

The brains of patients diagnosed with ASD, a condition notable for impaired communication and reciprocal social interaction, have been found to possess a disorganized cortex with irregular laminar cytoarchitecture[47]. To study the proliferative activity of fetal neural precursor and the migration of newborn neurons, pregnant mice received a single injection of bromodeoxyuridine (BrdU, 50 mg/kg), a thymidine analog that incorporates into the DNA of dividing cells during the S-phase of the cellular cycle, at GD14.5. These mice were then sacrificed at GD18.5 to collect embryonic brains for subsequent analyzes. Cortical development ordinarily progresses in an inside-out manner, with the neurons of the inner layers born first[48]. As gestation continues, newborn neurons migrate past these initial layers to sequentially inhabit the exterior layers of the cortex. Our results showed that maternal HFD had no significant impact on the proliferative activity of neural stem cells located in the ventricular and subventricular zones (VZ/SVZ) (Figs. S8a, b). Both the relative abundance of neurons and the distribution of cells within the cortical laminae are crucial to preserving the functional integrity of the neocortex[49]. Therefore, we counted cortical tissues to ascertain the distribution of BrdU-positive cells across 10 equally distributed laminar areas or "bins" (laminar distribution) (Fig. 5e). We observed a significant disruption in the laminar distribution of cells detected in the brains of mHFD fetuses, detailed in a depletion of cells born on E14.5 from the outer layers (bins 1 and 2) and an overrepresentation in the inner layers (bins 5-10) (Fig. 5f). We also observed a significant upsurge in BrdU-positive cell density across the entirety of the cortex in mHFD fetal forebrains (Fig. 5g–h). To confirm the arrest of neuronal migration in the deeper neocortical layers, cortical sections were immunostained for Brn2, a marker predominantly expressed in neurons situated in superficial layers (Fig. 5i). Consistent with the disrupted distribution of BrdU-positive cells in the fetal neocortex, the deeper layers revealed a substantial delay in Brn2-labeled cells (Fig. 5j). Notably, the maternal HFD did not show any discernible effects on the density of Brn2-positive neurons (Fig. 5k), suggesting that this dietary regimen did not influence the process of Brn2-positive neuron differentiation and maturation. Consistent with the improved social behaviors observed in male offspring (Fig. 2h–i), (+)-Naloxone administration effectively ameliorated the disruption of neuronal migration within the fetal neocortex (Fig. S8c–f). These results highlight the critical influence of MIA in mHFD fetal neurodevelopmental disorders. Mechanistic insights gleaned from RNA-seq analysis

https://doi.org/10.1038/s41467-025-57414-4

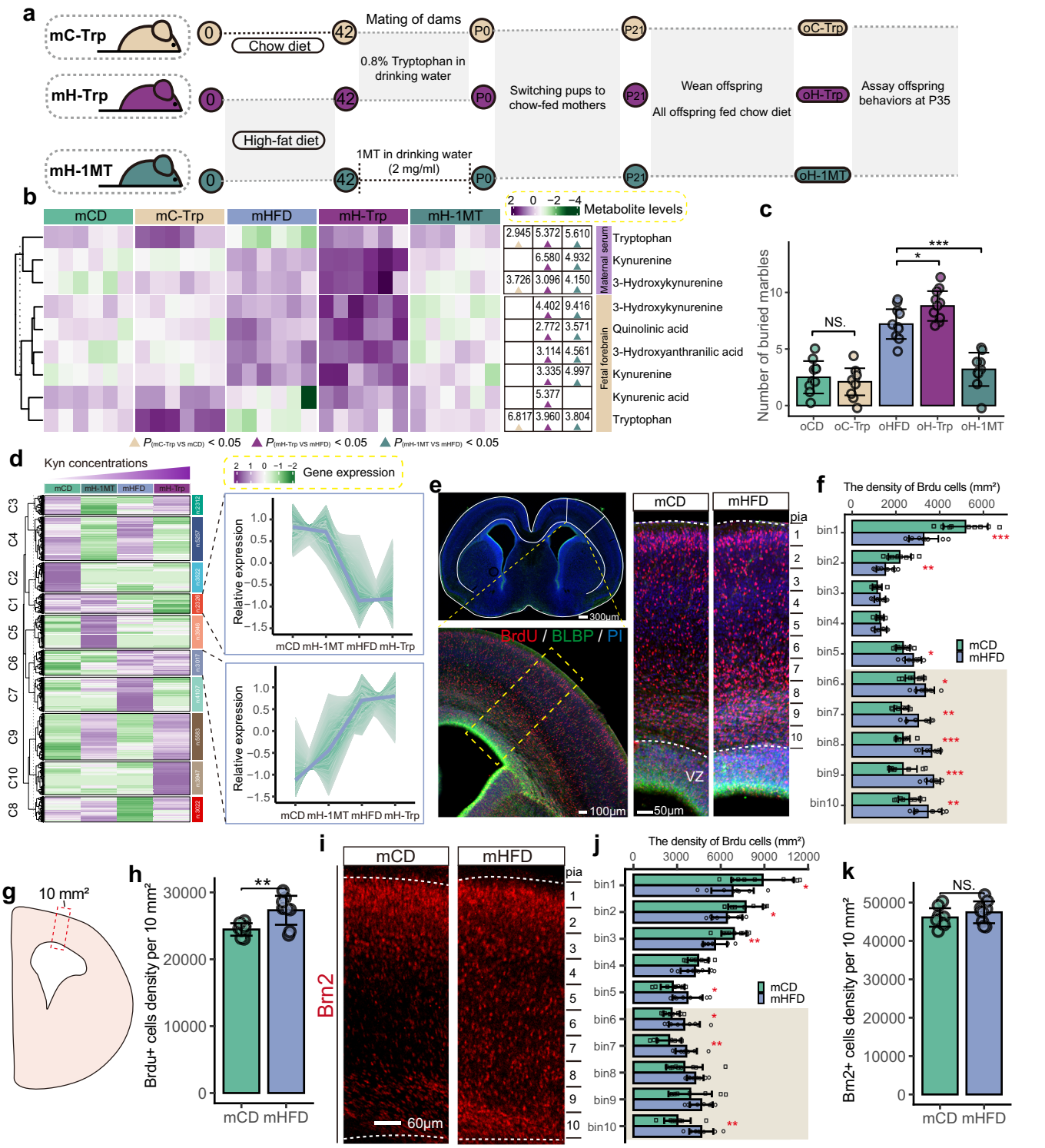

Fig. 5 | Maternal Trp modulation impacts embryonic brain development and offspring behavioral phenotypes. a Schematic of dietary Trp modulation. **b** Heatmap of Trp metabolite levels in maternal circulation and fetal brain ($n = 6$ mice/group). T-values were indicated (right). **c** Trp modulation affected male offspring's marble burying test ($n = 10$ mice, 10 litters/group; oCD vs oC-Trp, $t = 0.677$, $p = 0.507$; oHFD vs oH-Trp, $t = 2.717$, $p = 0.014$; oHFD vs oH-1MT, $t = 4.096$, $p = 0.000615341$). **d** Fuzzy c-means clustering of gene expression patterns in fetal forebrain ($n = 3$ mice/group). **e** Coronal brain section showing somatosensory and motor cortex assessment. **f** Density of BrdU-positive cells located in each laminar bin ($n = 9$ slices from 3 mice; bin1: $t = 4.694$, $p = 0.0002088483$; bin2: $t = 2.998$, $p = 0.009$; bin5: $t = 2.859$, $p = 0.011$; bin6: $t = 2.469$, $p = 0.025$; bin7: $t = 3.615$, $p = 0.002$; bin8: $t = 7.465$, $p = 9.243799e\text{-}07$; bin9: $t = 5.881$, $p = 1.814603e\text{-}05$; bin10: $t = 3.159$, $p = 0.006$). **g**, **h** Cortical cell density evaluation ($n = 9$ slices from 3 mice; $t = 3.653$, $p = 0.002$). Cortical columns were divided into ten equal-sized bins (**i**) and the number of Brn2-positive cells counted in each (**j**) $n = 9$ slices from 3 mice; bin1: $t = 2.389$, $p = 0.030$; bin2: $t = 2.408$, $p = 0.028$; bin3: $t = 3.244$, $p = 0.005$; bin5: $t = 2.314$, $p = 0.034$; bin6: $t = 2.168$, $p = 0.046$; bin7: $t = 3.146$, $p = 0.006$; bin10: $t = 3.999$, $p = 0.001$). Bin 10 represents the upper margin of the SVZ. **k** The density of Brn2-positive cells ($n = 9$ slices from 3 mice; $t = 1.079$, $p = 0.297$). Data are represented as mean ± SD. Statistical significance was assessed by the two-sided unpaired Student's t-test. Source data are provided as a Source Data file. Brdu bromodeoxyuridine, BLBP Brain lipid-binding protein, PI Propidium Iodide.

https://doi.org/10.1038/s41467-025-57414-4

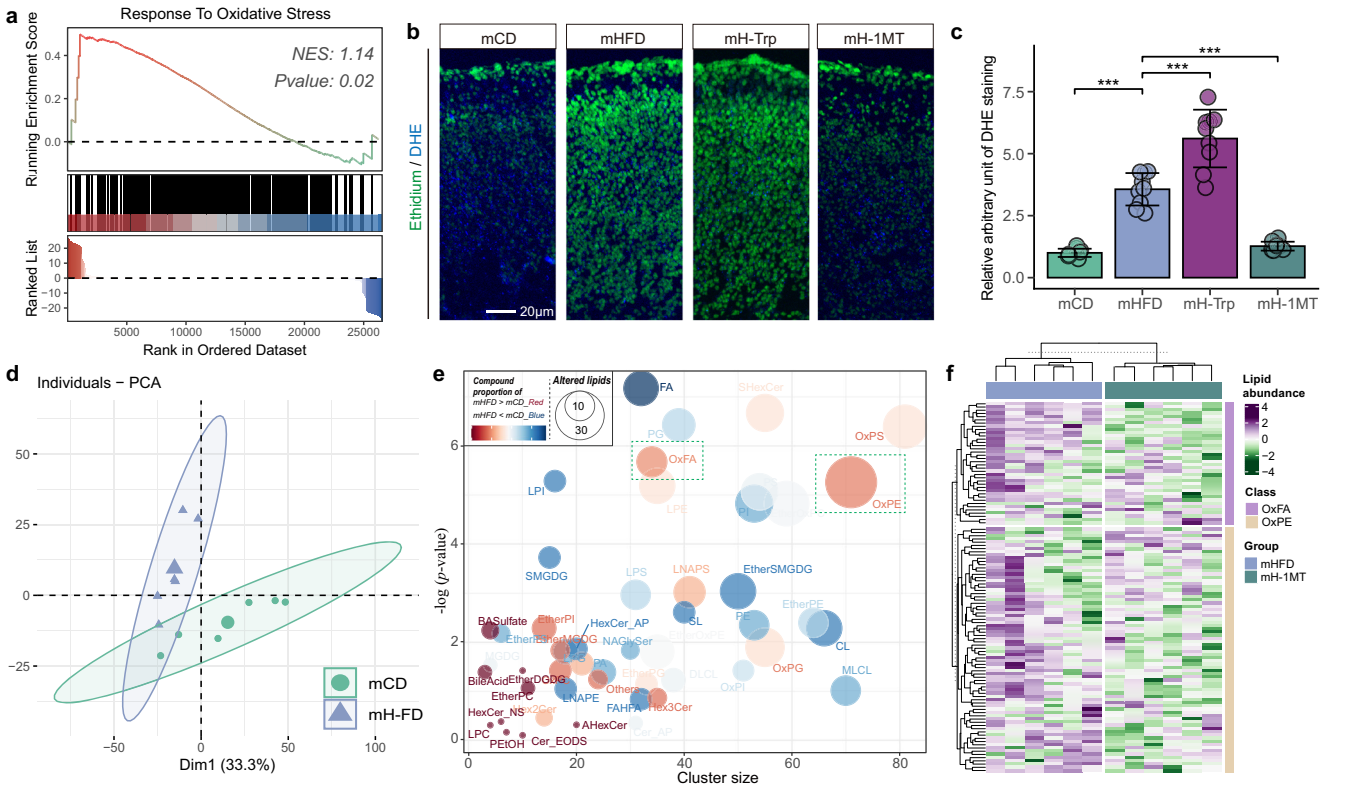

Fig. 6 | The dysregulated Kyn pathway causes oxidative stress in the fetal brain. **a** GSEA of activated oxidative stress pathway. **b** DHE staining of E18.5 fetal brain sections. **c** Statistical analysis of relative arbitrary unit of DHE staining ($n = 9$ slices from 3 mice; $F_{3,32} = 91.625$, mCD vs mHFD: $p = 2.2e\text{-}08$, mHFD vs mH-Trp: $p = 2.1e\text{-}06$; mHFD vs mH-1MT: $p = 2.3e\text{-}07$). Maternal HFD significantly altered lipid profiles in the fetal forebrain (**d**) and resulted in the overproduction of oxidized lipids (**e**) ($n = 6$ mice/group). **f** 1-MT treatment alleviated the accumulation of oxidized lipids in the embryonic brain ($n = 6$ for each group). Data are represented as mean ± SD. In **c** *p*-values were determined by ANOVA with Bonferroni's multiple comparison test. In **a** NES was calculated as described above. Statistical significance was determined using permutation testing (999 permutations), with FDR correction. In **c,** *p*-values were determined using one-way ANOVA, followed by Bonferroni's correction for multiple comparisons. In **d** PERMANOVA by Adonis was used to determine statistical significance ($F = 6.113$, $p = 0.007$). In **e** a one-sample Kolmogorov-Smirnov test was used to assess the null hypothesis that the *p*-values for lipids in a set follow a reference uniform distribution. FDR correction was performed for the set-level *p*-values. The nomenclature of lipid classes in (**e**) is available at http://prime.psc.riken.jp. Source data are provided as a Source Data file.

(Figs. 5d, S7a, b) informed our subsequent investigations toward the potential role of Kyn pathway dysregulation in fetal cortical abnormalities caused by maternal HFD-induced MIA. Examination of cortical development in mH-1MT fetuses revealed that the inhibition of the maternal Kyn pathway significantly counteracted the impaired neuronal migration in the embryonic neocortex (Fig. S8c–f), establishing causal links between MIA-dysregulated Kyn metabolism and consequential deficits in male offspring social behavior resulting from cortical disorganization.

Inhibition of the maternal Kyn pathway attenuates oxidative stress in the fetal brain

Most metabolites of the Kyn pathway have been observed to stimulate the release of synaptosomal glutamate (Fig. S9a), exerting detrimental effects via various mechanisms[50]. These include the production of reactive oxygen intermediates and the consumption of endogenous antioxidants[51]. Metabolomics carried out on both maternal serum and fetal forebrain revealed that the maternal HFD significantly perturbed the glutathione metabolism pathway (Figs. 3e, 4j), which is integral to antioxidant defense and cellular event regulation[52]. Moreover, an accumulation of reactive oxygen species (ROS) impacts various phases of cortical neuron development, including precursor cell proliferation, neuroblast migration and positioning, and neuronal maturation[53]. Corroborating the hyperactive Kyn pathway in the embryonic brain, GSEA results demonstrated a marked induction of oxidative stress response in the mHFD fetal forebrain relative to that of mCD (Fig. 6a). To conclusively ascertain ROS production levels in the brain, dihydroethidium (DHE) staining was implemented on the E18.5 fetal forebrain sections (Fig. 6b). Consistently, higher ROS levels were detected in the brain of the mHFD fetus compared to that of the mCD mice (Fig. 6c). Notably, the detrimental impact was amplified when Trp supplementation was introduced, causing an increase in ROS production in the mH-Trp fetal forebrain (Fig. 6b–c). A key mechanism by which ROS induces cellular disorders involves lipid peroxidation. The Brain tissues are susceptible to lipid peroxidation induced by ROS due to their high concentration of polyunsaturated lipids[54]. Untargeted lipidomics conducted on the E18.5 embryonic brain revealed a significant alteration in the lipid profiles resulting from maternal diet (Fig. 6d). Echoing the transcriptomic results (Fig. S9a), the chemical similarity enrichment analysis (ChemRICH) exposed a significant increase in oxidized lipid production, particularly oxidized fatty acid (OxFA) and oxidized phosphatidylethanolamine (OxPE), in the mHFD fetal forebrain (Fig. 6e). Notably, 1-MT administration effectively inhibited the oxidative stress response (Fig. S9b) and ROS accumulation (Fig. 6b–c) in the fetal brain. This protective effect was further confirmed by the reduced production of OxFA and OxPE in the mH-1MT fetal forebrain (Fig. 6f, S9b–d). Collectively, these findings suggest a potential connection between Kyn metabolism dysfunction-induced oxidative stress response and the impairment of embryonic brain development.

https://doi.org/10.1038/s41467-025-57414-4

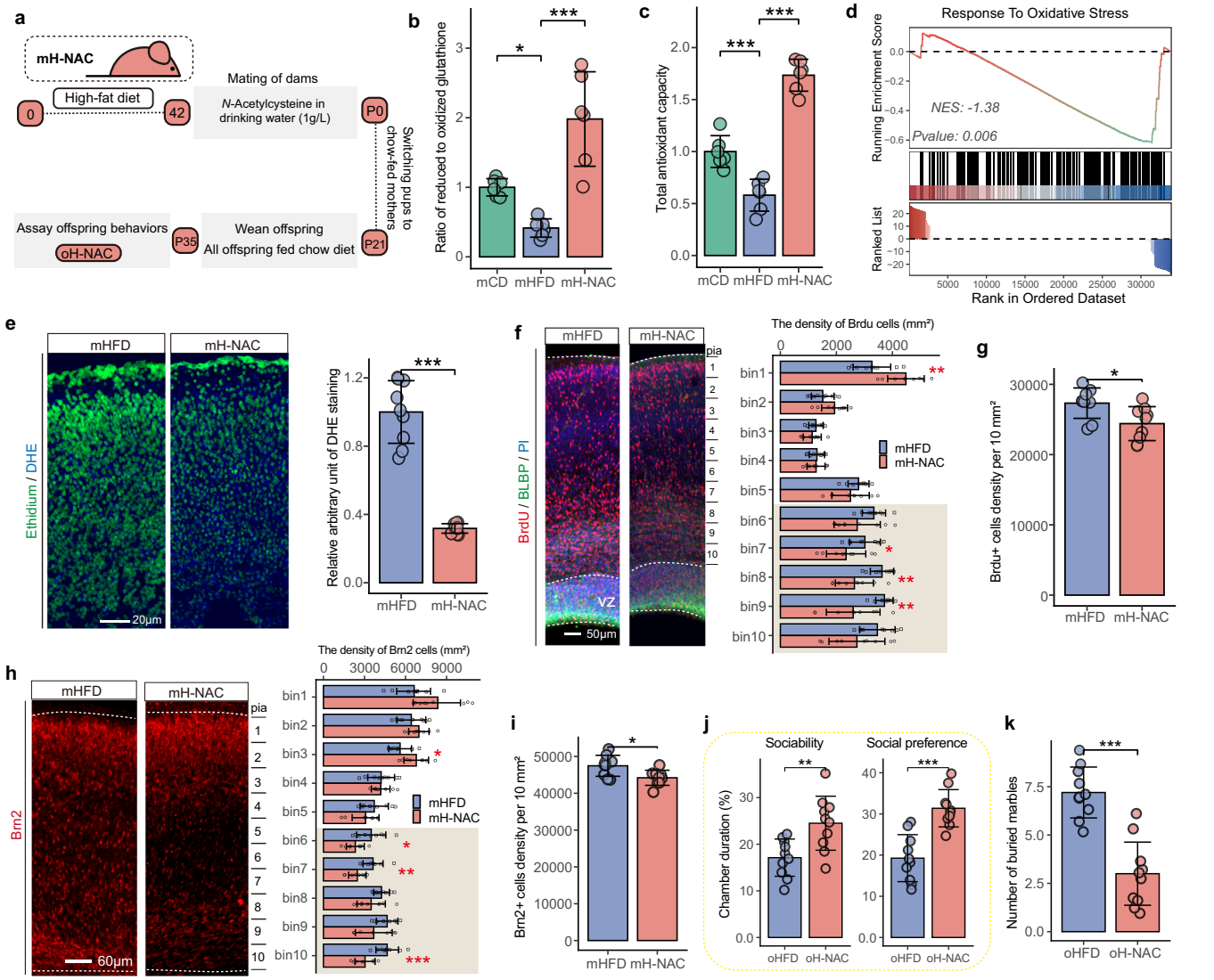

Fig. 7 | *N*-Acetylcysteine supplementation rescues oxidative stress-induced neuronal migration deficits and offspring behavioral dysfunction. a NAC supplementation schematic. **b** Measurement of the ratio of reduced to oxidized glutathione in the fetal brain ($n = 6$ mice/group; $F_{2,15} = 22.823$, mCD vs mHFD: $p = 0.045$, mHFD vs mH-NAC: $p = 1.41e\text{-}05$). **c** The total antioxidant capacity of the mH-NAC fetal brain was significantly improved ($n = 6$ mice/group; $F_{2,15} = 86.955$, mCD vs mHFD: $p = 0.000507$, mHFD vs mH-NAC: $p = 2.74e\text{-}09$). **d** GSEA of oxidative stress response ($n = 3$ for each group). **e** NAC inhibited superoxide production in the fetal brain ($n = 9$ slices from 3 mice; $t = 11.028$, $p = 1.064145e\text{-}09$). **f** Neuronal migration in fetal cortex ($n = 9$ slices from 3 mice; bin1: $t = 3.893$, $p = 0.001$; bin7: $t = 2.256$, $p = 0.038$; bin7: $t = 2.256$, $p = 0.038$; bin8: $t = 3.714$, $p = 0.002$; bin9: $t = 3.324$, $p = 0.004$). **h** NAC supplementation partially restored the distribution of Brn2-positive cells in the cerebral cortex ($n = 9$ slices from 3 mice; bin3: $t = 2.903$, $p = 0.010$; bin6: $t = 2.786$, $p = 0.013$; bin7: $t = 3.548$, $p = 0.003$; bin10: $t = 4.388$, $p = 0.0004013904$). A reduction in the total number of BrdU-positive (**g**) $t = 2.694$, $p = 0.016$) and Brn2-positive (**i**) $t = 2.782$, $p = 0.013$) neurons was observed in the mH-NAC fetal brain ($n = 9$ slices from 3 mice). **j** Offspring social behavior in three-chamber test ($n = 10$ mice, 10 litters/group; sociability: $t = 3.318$, $p = 0.004$; social preference: $t = 5.259$, $p = 4.47265e\text{-}05$). **k** Marble-burying test ($n = 10$ mice, 10 litters/group; $t = 6.332$, $p = 4.469088e\text{-}06$). Data are represented as mean ± SD. In **b**-**c**, *p*-values were determined by ANOVA with Dunnett's multiple comparison test. The rest of the statistical significance was assessed by the two-sided unpaired Student's t-test. Source data are provided as a Source Data file.

N-Acetylcysteine supplementation attenuates cortical neuronal migration deficits and social behavioral dysfunction in male offspring

Given the co-occurrence between redox dysregulation and cortical developmental shortfalls observed in the fetal brain, we aimed to ascertain whether reducing Kyn metabolites-induced oxidative stress might remediate embryonic brain development anomalies and associated behavioral disorders in the progeny. Corroborated the perturbs in the glutathione metabolism pathway in both maternal circulation and fetal brain revealed by metabolite enrichment analyzes (Figs. 3e, 4j), maternal HFD significantly decreased the ratio of reduced to oxidized glutathione and total antioxidant capacity in the fetal brain (Fig. 7b–c). As such, we supplemented the drinking water of HFD-fed mice with *N*-Acetylcysteine (NAC), a precursor of tissue glutathione synthesis, during pregnancy (mH-NAC, Fig. 7a)[55]. This intervention markedly improved the reduced glutathione ratio and enhanced total antioxidant capability (Fig. 7b-c), contributing to rectifying the redox imbalance present in the fetal brain of mothers on HFD. Additionally, this beneficial effect was further validated by the downregulated oxidative stress response pathway and minimized ROS production in the mH-NAC fetal forebrain (Figs. 7d–e, S10a). Subsequently, we noted significant shifts in lipid profiles in the mH-NAC fetal forebrain, marked by decreased oxidized lipid accumulation following maternal NAC administration (Fig. S10b–d). An inspection of fetal cortical development revealed that NAC supplementation moderated the arrest of neuronal migration in the cortical

deeper layers and the anomalous distribution of functional neurons (Fig. 7f, h). Interestingly, a minor drop in neuronal density was observed in the mH-NAC embryonic brain (Fig. 7g, i). These findings underscore the significant contribution of cellular redox equilibrium in preserving the structural and functional integrity of the neocortex. Advancing in line with these positive outcomes, social behavioral tests exhibited oH-NAC male offspring with superior sociability and social preference, and fewer buried marbles when compared to oHFD male offspring (Fig. 7j, k). In summary, our results validated the hypothesis that counteracting oxidative stress incited by Kyn metabolites is a viable strategy for correcting behavioral disorders in male offspring induced by a maternal HFD.

Discussion

Substantial research suggests that both genetic and environmental factors, along with their interplay, are instrumental in the etiology of neurodevelopmental disorders[56]. One notable observation alluded to repeatedly in epidemiological studies is that maternal obesity during pregnancy escalates the risk of neuropsychiatric disorders in offspring[57]. However, the fundamental mechanisms underlying this link, despite its clinical significance, are mostly not understood comprehensively. Our results provide perspectives into the mechanisms by which maternal consumption of HFD disrupts male offspring behavioral outcomes, highlighting the importance of maternal immune responses and metabolic regulation in modulating fetal brain developmental processes.

The human diet has drastically altered over the past century, transitioning from agriculture-based meals to high-calorie processed foods laden with saturated fatty acids[1]. This change is widely identified by researchers as a key factor in the rise of obesity and related metabolic disorders[58]. Furthermore, recent research has illuminated the role of diet in the regulation of the immune system and correlating inflammatory diseases[59]. Our latest report stipulates that a consistent HFD impairs mitochondria in the colonocytes, thus enhancing access for host-derived respiratory substrates to intestinal pathogens, subsequently leading to an increase in *Escherichia coli* (*E.coli*)-derived LPS concentrations in circulation, initiating systemic inflammation[21]. When confronted with environmental hazards, an inflammatory response is triggered to provide protection against pathogens and facilitate tissue regeneration, thereby preserving cellular homeostasis[60]. However, excessive or erroneously regulated inflammation can result in detrimental imprinting of the immune system, thereby increasing susceptibility to chronic diseases[61]. Rodent studies further suggest that heightened inflammation during pregnancy due to bacterial infections or other inflammatory triggers has been correlated with neurodevelopmental and psychiatric disorders in the offspring[12–14]. While the mechanisms of MIA-elicited impairments are largely unknown, prenatal administration of LPS has been linked to inflammatory cytokine production in maternal circulation and the fetal brain[62]. Recent mouse studies indicate a key role for IL-17a in inducing LPS-based, autism-like behaviors[63]. Similarly, our study has observed that (+)-Naloxone treatment can curb HFD-induced maternal inflammation, characterized by the down-regulation of the IL-17 signaling pathway, along with the production of IL-17a and IL-17f, thereby rectifying social behavioral deficiencies in male offspring (Fig. 2f–i). IL-17a has drawn attention due to its direct or indirect effects on brain cells and neurological and neuromodulatory phenotypes[64]. For instance, a high-salt diet increased IL-17a production resulting in brain endothelial damage and cognitive dysfunction, as seen through altered behaviors[65]. IL-17a has also been suspected to cause anxiety- and depression-like behaviors in mice[66]. Although certain maternal cytokines have been pinpointed as essential mediators of MIA on disease-related phenotypes in offspring, the underlying mechanisms of brain development alterations caused by these maternal cytokines remain unclear.

The correlation between metabolism and immunity has been documented since the 1960s[67]. Recent advancements in immunometabolism research have further elucidated the intricate relationship between host metabolic processes and immune responses[68]. Notably, the presence of infection-induced proinflammatory cytokines has the capacity to influence both amino acid and lipid metabolism, emphasizing their pivotal role in the metabolic reprogramming of the host[69]. Therefore, we proposed a hypothesis that MIA-induced metabolic stress might play a role in offspring behavioral deficits associated with maternal HFD (Fig. 8). Comprehensive analysis of proinflammatory cytokines and metabolites revealed that maternal HFD significantly disrupted Trp-Kyn metabolism in the maternal circulation (Fig. 3c–f). A noteworthy fact is that over 95% of free Trp undergoes degradation via the Kyn pathway, forming metabolites with various biological activities in immune response and neurotransmission[36]. IDO1, the main rate-limiting enzyme of the Kyn pathway, is expressed in numerous cell types, such as microglia, and its activity is regulated by proinflammatory cytokines (e.g. IL-17) and TLR ligands[36,70,71]. Activation of the Kyn pathway triggers a negative feedback mechanism that mitigates the inflammatory response[72]. However, given that many Kyn metabolites are neuroactive, this protective effect may be counteracted by increased production of neurotoxic metabolites of the Kyn pathway (e.g., 3-HK and Quin)[73]. This fact provides a plausible explanation as to why extra supplementation of Trp to HFD-fed pregnant mice intensifies the severity of stereotypical behaviors in their offspring (Fig. 5c). Notably, the CNS receives ~60% of Kyn from the periphery, facilitated by transport across the blood-brain barrier[74]. Moreover, akin to Trp and Kyn, 3-HK can cross the blood-brain barrier, contributing to Quin production in microglia, while also having the potential to cause more direct harmful effects linked to neurodevelopmental abnormalities[75]. Consequently, abnormal accumulation of Kyn metabolites was identified in the fetal brain of mHFD mice, showing a strong correlation with maternal serum levels (Figs. 5b, S3b–e). The metabolic process of Kyn in the brain is largely directed by the activity of microglia, which begin to populate the brain at E8.5[76]. Microglia in the developing brain are morphologically and functionally unique compared to those in the adult brain[76]. Inflammatory insults are shown to hasten the maturation and functional differentiation of microglia[77]. Morphological analysis revealed that microglia in the cerebral cortex of the mHFD fetus reveal a more complex profile (Fig. 4b–c), indicative of a hyperactivated phenotype which aids in converting Kyn to Quin. Inhibition of MIA via (+)-Naloxone or direct suppression of IDO1 activities by 1-MT significantly mitigated the Kyn pathway in fetal brain and social performance in adolescent offspring (Figs. 2h–i, 5b–c; S3b, S5a–c), demonstrating the critical role of MIA-induced metabolic stress in offspring behavioral dysfunction.

The mammalian neocortex, a highly organized and complex structure, plays significant roles in numerous higher cognitive, emotional, and sensorimotor functions[78]. It is vital to maintain proper regulation during neuronal migration from the deeper part of the developing brain towards the pial surface, as impairments in this process could lead to disorders such as brain malformation or psychiatric illnesses[79]. The published data from studies involving children with ASD exhibit abnormal laminar cytoarchitecture and cortical disorganization of neurons, especially in the prefrontal and temporal cortical tissue[80,81]. Moreover, a mouse model of MIA exposed to viral infection suggests that a distinctive cortical phenotype may drive observable behavioral anomalies in offspring[82]. The gestation period, a critical time for the rapid establishment of foundational structures and neural networks in the fetal brain, also represents a period of particular vulnerability[83]. However, the effects of prenatal maternal HFD on the development of the fetal brain *in utero* have been sparingly reported. Conventional wisdom affirms that MIA incited by bacterial or viral infection inhibits axon guidance, neurogenesis, and cytoskeleton genes while promoting genes involved in translation, cell cycle, and

https://doi.org/10.1038/s41467-025-57414-4

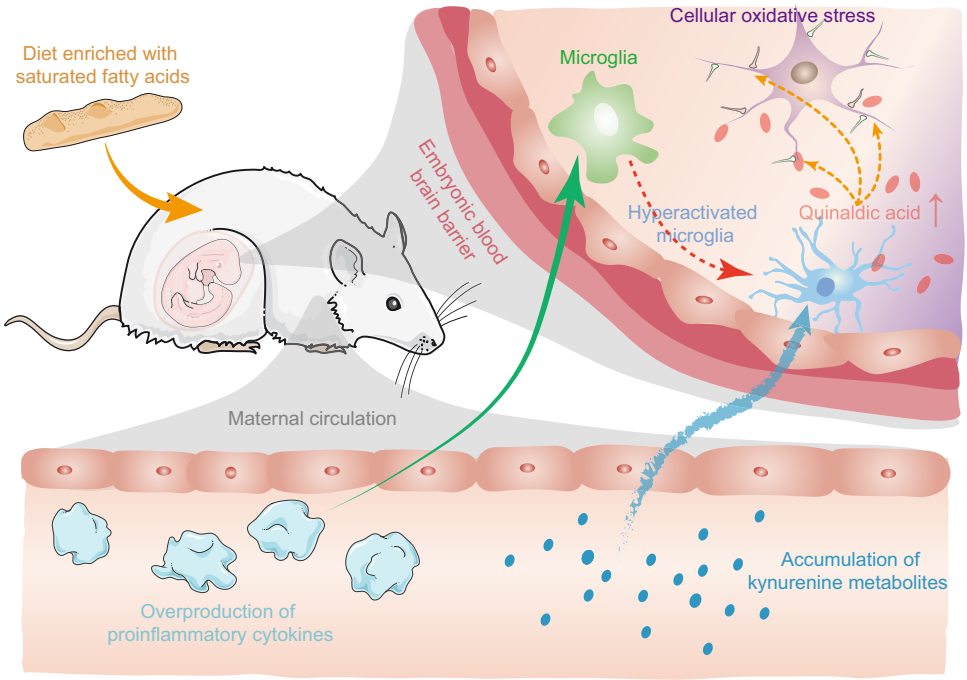

Fig. 8 | Schematic diagram of the mechanism underlying maternal HFD-induced offspring behavioral dysfunction. Prenatal HFD enhanced maternal inflammatory activities, promoting the accumulation of Kyn metabolites in the maternal bloodstream. Most Kyn metabolites readily cross the blood-brain barrier. Concurrently, maternal HFD-associated MIA stimulated the overactivity of microglia within the fetal brain, culminating in the transformation of Kyn into the neurotoxic compound Quin. An overabundance of Quin subsequently induced an oxidative stress response, which impairs neuronal migration within the fetal neocortex and postnatal social behavioral phenotypes.

DNA damage processes[84]. Transcriptomic analysis in our study revealed a strong correlation between excessive Kyn production and hampered neuronal development and migration in the fetal brain (Fig. 5d), suggesting that dysfunctional Kyn metabolism may be the critical factor in causing MIA-induced cerebral developmental deficits among mHFD progeny. Neurotoxic Kyn metabolites, such as Quin and 3-HK, have been demonstrated to interfere with neurodevelopment in several animal models by elevating extracellular levels of glutamate, obstructing glutamate uptake by astrocytes, depleting endogenous antioxidants, and triggering ROS and lipid peroxidation[75]. Simultaneously, recent research affirms that oxidative stress contributes to ASD pathogenesis[85]. Our findings suggest that maternal Trp modulation regulates the oxidative stress response and neurodevelopment within the fetal brain (Figs. 6a–c, 7f–i), which offers a mechanistic understanding of maternal HFD-induced cortical disorganization. Moreover, case-control studies have observed that children with ASD show aberrant plasma metabolite levels in the glutathione redox pathway, typically showcasing a decrease in reduced glutathione and an increase in oxidized glutathione disulfide[86]. Metabolomics analysis results indicate that HFD disrupts both maternal and embryonic glutathione metabolism (Figs. 3e, 4j), potentially aggravating the oxidative stress impairment caused by an overabundance of Kyn metabolites in the fetal brain. Notably, introducing NAC to HFD-fed pregnant mice has proven effective in restoring the balance in glutathione redox and mitigating ROS production in the fetal brain (Fig. 7b–e), thereby ameliorating social behavioral deficits in the offspring. These results further corroborate the hypothesis that the dysregulated Kyn pathway-induced oxidative stress response in the fetal brain is vital for the abnormal behavioral phenotype of HFD offspring.

The current study bears several limitations that warrant acknowledgment. Previous research demonstrates that male offspring of MIA, as opposed to females, present heightened vulnerability to neurodevelopmental disorders[16]. This fact informed our choice to select male offspring for this study. Therefore, further follow-up evidence is needed to reveal the specific mechanisms by which maternal diet affects female offspring. Furthermore, although both the inhibition of maternal Kyn metabolism and NAC supplementation have been shown to alleviate oxidative stress impairment in the mHFD embryonic brain, and to mitigate postnatal behavioral anomalies in offspring, the need remains to further affirm the health risks of these interventions. Lastly, while glutamate acts as a catalyst of Kyn metabolite-induced neurotoxicity, it also governs neuronal development and migration. In the embryonic brain, glutamate manages the radial migration of pyramidal neurons primarily through NMDA receptors and controls the tangential migration of inhibitory interneurons by activating non-NMDA and NMDA receptors[87]. Therefore, understanding whether the disorganized laminar distribution in mHFD embryonic brains may be due to irregular glutamate gradients in cerebral tissue is critical for specifying preventive and therapeutic strategies.

Our study reveals that dysregulated Kyn metabolism, linked to maternal inflammatory events, plays a significant role in the behavioral deficits observed in the male offspring of mothers with obesity. This occurs via the underlying mechanism of Kyn metabolite accumulation in the fetal brain, which disrupts cellular redox reactions and thereby interferes with neuronal migration and distribution in the cerebral cortex. Moreover, our data indicates that attenuating maternal immune activity or manipulating the Kyn pathway during pregnancy effectively mitigates social behavioral deficits in male offspring. Taken together, these findings provide investigational avenues for preemptive therapies targeting maternal diet-mediated neurodevelopmental disorders in male offspring, and indicate that amelioration of MIA-induced metabolic stress during pregnancy is a potentially timely and controllable approach to the treatment of neurodevelopmental disorders.

Methods

Animal experiments

This study was conducted in strict accordance with the ethical guidelines of the College of Veterinary Medicine, Northwest A&F University (Approval No.IACUC2023-0301). The Ethics Committee approved all experimental protocols, which adhered to the "Guide for the Care and Use of Laboratory Animals: Eighth Edition". Female C57BL/6 J mice, aged 4 weeks, were acquired from SPF Biotechnology Co., Ltd. in Beijing, China. Mice were housed in a controlled environment with a 12-hour light/dark cycle, room temperature maintained between 22 °C and 24 °C, and relative humidity of 50-60%. Prior to the commencement of the experiments, mice were fed with a standard chow that served as the control diet. Throughout the study, both the animal care staff and experimenters were blinded to the treatment groups. Mice were given unrestricted access to either the standard chow diet or a high-fat diet, and water was available ad libitum.

To investigate the effects of maternal HFD on offspring behavior, female mice at 6 weeks of age were randomly divided into two dietary groups (n = 22 for each group) for a period of 6 weeks: a standard chow diet (Cat. No. XTC01WC; kal%: 10% fat, 73% carbohydrates, 17% protein; gm%: 5% fat, 65% carbohydrates, 20% protein) and a high-fat diet (Cat. No. XTHF40-1; kal%: 63% fat, 20% carbohydrates, 17% protein; gm%: 40% fat, 30% carbohydrates, 23% protein). Diets were obtained from Jiangsu Xietong Pharmaceutical Bioengineering Co., Jiangsu, China, and stored at -20 °C. Timed pregnancies were established through overnight mating, with the presence of a seminal plug indicating embryonic day 0.5 (E0.5). Recent studies have shown that fetal sex influences the incidence of psychiatric and neurodevelopmental disorders, with susceptibility differing between male and female offspring[88–90]. These findings align with the results of human epidemiological studies, which indicate a higher prevalence of autism in males compared to females[33]. Moreover, model animal studies have demonstrated that the outcome of MIA is influenced by sex differences in offspring, with male offspring exhibiting greater susceptibility to maternal inflammation[29,76]. Therefore, this study focuses on the effects of maternal diet-induced shifts in immuno-metabolic homeostasis on the brain development and behavioral phenotypes of male offspring. Offspring sex was determined via PCR using *sry* gene-specific primers: 5′-ACAAGTTGGCCCAGCAGAAT-3′, and 5′-GGGATATCAACAGGCTGC CA-3′[15]. We used the method described by Jessica et al. to avoid litter effects and minimize false replicates[91]. This involved randomly selecting one animal from each litter for each test.

To elucidate the impact of maternal pre- and post-pregnancy high-fat diets on behavioral outcomes in offspring, a cross-fostering experiment was conducted in which newborns were exchanged between mothers consuming a standard diet and those consuming a high-fat diet. To assess the impact of maternal postnatal high-fat diet on the social behavior of offspring, the offspring of normal diet-fed mice were switched at birth to high-fat diet-fed mothers (mC-H, n = 18), with litters between 1 and 5 days old (which were removed). In the remaining group, newborns were transferred to standard-diet mothers. To explore the role of HFD-induced inflammation on male offspring behavior, the TLR4 antagonist (+)-Naloxone (5 mg/kg, Cat. No. N822820)[32] was dissolved in saline and administered to HFD-fed mice during pregnancy by daily gavage (mHFD-Nalo, n = 22). To investigate further the role of upregulated IL-17 expression in maternal HFD-induced social behavioral deficits in offspring, we inhibited the IL-17 signaling pathway by tail vein injection of IL-17a antibody in pregnant mice. Pregnant mice were injected with IL-17a antibody (mH-Anti-IL-17a, n = 18) or IgG1 isotype control (mH-IgG1, n = 18) (100 μg/mouse every 2 days) from GD0.5. The IL-17a antibody and IgG1 isotype control were purchased from Bio X Cell China (Cat. No. BE0173, Cat. No. BE0083). To examine the impact of maternal Trp modulation on male offspring behavior, pregnant mice on either a control diet (mC-Trp, n = 18) or an HFD (mH-Trp, n = 18) received 0.8% Trp (Cat. No. L818799) in their drinking water[45]. Additionally, we investigated the involvement of maternal Kyn metabolites in social behavioral deficits by administering 1-methyl tryptophan (2 mg/ml in drinking water, Cat. No.M813887)[44], an indoleamine 2,3-dioxygenase 1 (IDO1) inhibitor, to HFD-fed pregnant mice (mH-1MT, n = 18). Lastly, *N*-Acetylcysteine (1 g/L, Cat. No. N872752)[92] was supplied in drinking water to pregnant mice on an HFD (mH-NAC, n = 18) to examine if inhibiting maternal HFD-induced oxidative stress could mitigate embryonic brain development impairments and subsequent behavioral issues in progeny. All chemicals were sourced from Shanghai Macklin Biochemical Co., Ltd, Shanghai, China. To analyze fetal neural precursor proliferation and neuronal migration, we randomly selected three pregnant mice per group and administered a single injection of bromodeoxyuridine (BrdU, 50 mg/kg; Thermo Fisher Scientific, Cat. No.B23151) at E14.5. At E18.5, the mice were euthanized humanely using pentobarbital sodium (0.56% v/v, 10 mg/ml) and cervical dislocation, after which biological samples were collected.

Metabolomics

The sample extraction and instrumental analysis procedures were conducted in accordance with established protocols[93]. Serum samples (20 μL) were extracted using ice-cold methanol containing L-tryptophan-2,3,3-d3 internal standard (100 ng/ml). Following protein precipitation and centrifugation (15,000×g, 10 min), supernatants were concentrated via SpeedVac. For E18.5 fetal brain tissue analysis, samples (20 mg) underwent homogenization in methanol using a TissueLyzer (70 Hz, 5 min), followed by -20°C incubation and centrifugation (18,000×g, 10 min). All dried extracts were reconstituted in acetonitrile:water (2:98, v/v) prior to analysis.

Metabolomic analysis was performed on a Triple TOF 5600+ mass spectrometer, using a Waters Acquity UPLC HSS T3 column (100 Å, 1.8 μm, 2.1 mm × 100 mm) for chromatographic separation. The mobile phases consisted of 0.1% formic acid in water (solvent A) and 0.1% formic acid in acetonitrile (solvent B), delivered at 0.4 mL/min and 40°C. A 15-minute gradient was employed, starting at 2% B (1 min), ramping to 15% B (2 min), 50% B (3 min), 98% B (1.5 min, held for 4 min), and back to 2% B (0.1 min) for equilibration. Positive ionization using heated electrospray ionization (HESI) was applied with the following settings: sheath gas 60 L/min, auxiliary gas 10 L/min, sweep gas 1 L/min, spray voltage 2.75 kV, capillary temperature 325°C, and auxiliary gas heater temperature 400 °C. MS1 acquisition covered 80-1,000 Da at 70,000 resolution (FWHM at 200 Da). MS/MS was acquired in parallel reaction monitoring (PRM) mode with normalized collision energies of 10, 50, and 100, resolution of 17,500 (FWHM), AGC target 2e5, and max IT 50 ms.

Mass spectral data processing was performed using R (version 4.1.3). MS1.wiff files were converted to.mzXML and MS2.wiff to.mgf formats using ProteoWizard MS Convert tool. The converted files were then analyzed in R using TidyMass[94] to generate master peak tables, which aligned features across all samples. Metabolite annotation was performed using the Human Metabolome Database (HMDB)[95]. Differential metabolite analysis was identified with the DESeq2 package, and quantitative metabolite set enrichment analysis (qMSEA) was conducted employing the MetaboAnalystR package to elucidate the biological functions of the altered metabolites[96].

UID RNA-sequencing of colonic tissues

The E18.5 fetal forebrain was excised and preserved in liquid nitrogen for RNA sequencing. A 50 mg tissue sample was subjected to RNA isolation, performed by Seqhealth Technology Co., Ltd. (Wuhan, China), which included RNA extraction, library construction, and sequencing. Total RNA was purified from the tissue using TRIzol Reagent (Invitrogen) following the Chomczynski protocol. DNA contamination was removed via DNaseI treatment. RNA purity was assessed by the A260/A280 ratio using a Nanodrop™ OneC

spectrophotometer, and RNA integrity was checked with 1.5% agarose gel electrophoresis. RNA concentration was determined using a Qubit 3.0 fluorometer with the Qubit™ RNA Broad Range Assay kit (Life Technologies).

For library preparation, 2 μg of total RNA was processed with the KC-Digital™ Stranded mRNA Library Prep Kit for Illumina® (Wuhan Seqhealth Co., Ltd.), which incorporated an 8-base UMI to reduce PCR and sequencing biases. Library fragments (200-500 bp) were selected, quantified, and sequenced on a DNBSEQ-T7 sequencer (MGI Tech Co., Ltd.) using the PE150 model.

Initial raw sequencing data were processed with Trimmomatic to remove low-quality reads and adapter sequences[97]. Decontamination involved clustering reads by UMI, creating sub-clusters with >95% sequence similarity through pairwise alignment, and generating consensus sequences. These refined sequences were used for RNA-seq analysis. Sequences were aligned to the mouse reference genome using STAR. Reads mapping to gene exons were counted with FeatureCounts (Subread-1.5.1)[98], facilitating RPKM calculations. Differential gene expression was analyzed using DESeq2 in R, and Gene Set Enrichment Analysis (GSEA) was performed using ClusterProfiler and GseaVis packages, ranking genes by differential expression.

Lipidomics analysis

Lipidomics analysis was performed following an established protocol for sample extraction and instrumental analysis[98]. To extract lipids from the fetal forebrain, 20 mg of tissue was homogenized in 600 μL methanol using a bead pulverizing machine at 6000 rpm for 15 seconds (repeated twice). The homogenate was transferred to a 2 mL glass vial, and 600 μL chloroform was added, followed by vortexing for 10 seconds. The mixture was incubated for 60 minutes at room temperature, then 200 μL Milli-Q water was added, and the solution was vortexed again for 10 seconds. After a 15-minute incubation, the mixture was centrifuged at 2000g for 10 minutes at 20°C. The supernatant was carefully transferred into LC/MS vials for analysis.

Untargeted lipidomics analysis was carried out using an ACQUITY UPLC system coupled with a QTOF-MS (TripleTOF 5600 +) instrument. Chromatographic separation was achieved on an Acquity UPLC Peptide BEH C18 column at 45 °C with a flow rate of 0.3 mL/min. The mobile phase consisted of two solvents: (A) acetonitrile, methanol, and water in a 1:1:3 (v/v/v) ratio with 5 mM ammonium acetate and 10 nM EDTA, and (B) pure isopropanol containing 5 mM ammonium formate and 10 nM EDTA. The gradient started at 0% B, held for 1 minute, increased to 40% B over 5 minutes, reached 64% B at 7.5 minutes, maintained for 4.5 minutes, then increased to 82.5% B at 12.5 minutes, 85% B at 19 minutes, peaked at 95% B at 20 minutes, and returned to 0% B at 20.1 minutes, for a total run time of 25 minutes. Sample temperature was kept at 4 °C. MS analysis was performed in high sensitivity mode with data-dependent MS/MS acquisition. The mass ranges for MS1 and MS2 were m/z 70–2000, with accumulation times of 250 ms for MS1 and 100 ms for MS2. The collision energy was set at 40 eV with a 15 eV spread, and the cycle time was 1300 ms. Optimal ionization and detection conditions were achieved using APCI positive/negative calibration for automatic mass calibration. Differentially expressed lipids were identified using the DESeq2 package. Chemical similarity enrichment analysis (ChemRICH) plots were generated to visualize lipid variations across chemical classes[99].

Three-chamber social-behavior assay

Male mice, aged 5 weeks, underwent a three-chambered social-approach test to assess their social behavior. The day before testing, the mice were placed in a 50×35×30 cm three-chambered arena containing empty containment cages for a 10-minute acclimation period. On the test day, the mice explored the same environment with the empty cages for 5 minutes before being restricted to the central chamber. One peripheral chamber contained a novel C57BL/6 male mouse as a social stimulus, and the opposite chamber contained an inanimate object of similar size. After removing the barriers between the chambers, the mice were allowed to explore for 10 minutes. Their interactions, including sniffing and approach behaviors within a 2 cm range, were recorded. Video analysis using SMART VIDEO TRACKING software (Panlab, Spain) was employed to track the object exploration time and overall movement. A social preference index was calculated by comparing the time spent exploring the social stimulus to the total exploration time. The arenas and objects were sanitized between trials, and different social stimuli from various home cages were used to control for potential olfactory confounds.

Marble-burying Test

Male mice, aged 5 weeks, were placed in a 40×20 cm^2 experimental arena with 3 cm of bedding and 20 glass marbles arranged in five rows of four equidistantly spaced marbles. After a 15-minute exploration period, the mice were removed, and the number of buried marbles was recorded. Marbles were considered buried if more than 50% of their surface area was covered by bedding. Each buried marble was assigned a marble-burying index of 1, and any marble with less than 50% coverage was scored as 0.

Olink proteomic analysis

Serum proteins were measured using the Olink® Target 96 Mouse Exploratory Panel* (Olink Proteomics AB, Uppsala, Sweden) according to the manufacturer's instructions. The employed Proximity Extension Assay (PEA) technique, which has been extensively documented in prior literature, allows for the concurrent analysis of 92 analytes with just 1 μL of sample. Briefly, the assay employs two oligonucleotide-labeled antibody probes that specifically bind to their respective protein targets. Upon proximal binding of the probes to the target protein, the attached oligonucleotides undergo hybridization. This process is further amplified by the introduction of DNA polymerase, triggering a proximity-induced polymerization reaction that produces a unique PCR-readable DNA sequence. The amplified DNA is then quantified using a microfluidic real-time PCR instrument (Signature Q100). Following this, data undergo rigorous quality control measures that include normalization against both an internal extension control and an inter-plate control to correct for variations within and between runs. Quantitative results are reported as Normalized Protein Expression (NPX) values, which are arbitrary units expressed on a log2-scale that directly correlates with the protein expression levels - higher NPX values indicate greater protein concentrations.

For the subsequent analysis, the DESeq2 package within R was employed to pinpoint differentially expressed serum proteins[100]. Additionally, Metascape enrichment network analysis aided in identifying perturbed biological pathways[101]. Proteins sorted by their expression discrepancies were further examined using Gene Set Enrichment Analysis (GSEA) with the R packages ClusterProfiler[102] and GseaVis (https://github.com/junjunlab/GseaVis).

Social behavioral assay

Animals from the same litter often share more similarities than those from different litters. This variation, known as 'litter effects', can impact results alongside experimental factors[103]. Jessica et al. provide guidance to help scientists reduce the impact of litter effects and improve the rigor and reproducibility of studies on neurodevelopmental disorders using rodent models[91]. Therefore, only one animal per litter, randomly selected, was used for behavioral analysis. Male offspring (5-week-old) were tested for sociability using a three-chamber social approach paradigm and marble burying test. The procedure for testing social behavior was performed following previous reports[16]. Detailed methodologies are described in the Supplementary Materials section.

Immunofluorescence assay

The fetal brain was fixed in 4% paraformaldehyde, followed by sectioning at a thickness of 50 μm using a Leica Biosystems Vibratome. The following primary antibodies were used in this study: Rabbit anti-Iba1 (Abcam, Cat. No. ab178846) at a dilution of 1:500, Rabbit anti-BrdU (Abcam, Cat. No. ab308341) at a dilution of 1:800, and Mouse anti-Brn2 (Abcam, Cat. No. ab243045) at a dilution of 1:500. After blocking with 5% normal donkey serum in PBS for 1 hour at room temperature, tissue sections were incubated overnight at 4 °C with the primary antibodies in PBS containing 0.3% Triton X-100. Following primary antibody incubation, sections were washed three times with PBS and incubated with appropriate secondary antibodies for 2 hours at room temperature. Immunofluorescent images were acquired using a confocal microscope. All procedures were carried out in the dark to protect from photobleaching.

Quantification and morphological analysis of microglia

Microglial density was quantified using an Olympus FV3000 laser-scanning confocal microscope (Japan) at 10x magnification. Iba1-positive cells were counted in the defined regions of interest, and the number of cells per unit area was calculated. For morphological analysis, microglia were imaged using a 20x objective, and z-stack images were acquired with 0.2 μm intervals. The acquired images were analyzed for morphology using ImageJ software. Skeletonization of microglial processes was performed using the "Skeletonize" plugin, and fractal dimension was calculated using the "Fractal Analysis" plugin in ImageJ.

RNA extraction and *q*RT-PCR

Total RNA was extracted from tissue samples using the RNeasy Mini Kit (Qiagen, Cat. No. 74104), following the manufacturer's instructions. RNA concentration and purity were assessed using a NanoDrop spectrophotometer. cDNA was synthesized from 1 μg of RNA using the SuperScript IV Reverse Transcriptase kit (Thermo Fisher Scientific, Cat. No. 18090050), following the manufacturer's protocol. Quantitative PCR was performed on a QuantStudio 5 Real-Time PCR System (Thermo Fisher Scientific) using SYBR Green PCR Master Mix (Thermo Fisher Scientific, Cat. No. 4309155). The following primers were used for the amplification: GAPDH (forward 5′-AGGTTGTCTCCTGCGACT GCA, reverse 5′-GTGGTCCAGGGTTTCTTACTCC) and KMO (forward 5′-ATGGCATCGTCTGATACTCAGG, reverse 5′-CCCTAGCTTCGTACACAT CAACT).

Each PCR reaction was performed in triplicate in a 20 μL volume containing 10 μL of SYBR Green Master Mix, 0.5 μM of each primer, and 1 μL of cDNA template. The following PCR conditions were used: 95 °C for 10 minutes, followed by 40 cycles of 95 °C for 15 seconds, 60 °C for 1 minute. A melting curve analysis was performed after the amplification cycles to verify the specificity of the amplicons. Relative gene expression was calculated using the $2^{-\Delta\Delta Ct}$ method, normalizing to GAPDH as the housekeeping gene.

Detection of serum endotoxin

Endotoxin concentrations in the serum were quantified with the LPS ELISA Kit (Wuhan Fine Biotech Co., Ltd, Wuhan, China, Cat. No. EU3126), following the provided manual.

Detection of ROS production

For ROS quantification, dihydroethidium (DHE) (Beyotime, Cat. No. S0063) staining was applied; E18.5 fetal brain sections (5 μm) were incubated with 30 μmol/L DHE in obscurity for 30 minutes at ambient temperature, in accordance with the manufacturer's protocol. Fluorescence microscopy (ZEISS, Germany) was utilized to capture images. The DHE fluorescence intensity was measured and quantified using Image J software (Version 1.83, National Institutes of Health, USA).

Detection of maternal cytokine and chemokine levels

The maternal serum levels of IL-17a and CCL5 were determined by ELISA kits (Multisciences (Lianke) Biotech Co., Ltd, Hangzhou, China, Cat. No. EK2129/2, EK217/2) in accordance with the provided manual.

Total antioxidant capacity test

The T-AOC Assay Kit (Beyotime, Cat. No. S0121) was employed to evaluate the total antioxidant capacity of E18.5 fetal brains, strictly following the kit-specific instructions.

Weighted correlation network analysis

Weighted correlation network analysis (WGCNA) was performed using the WGCNA R package. To construct signed co-expression networks, serum metabolite datasets were used as input. First, data preprocessing was performed, including filtering for low-variance metabolites and normalization. The soft thresholding power was determined using the "pickSoftThreshold" function to ensure a scale-free network. A signed topological overlap matrix (TOM) was calculated using the "TOMsimilarity" function, and hierarchical clustering of the metabolites was performed based on the TOM. Modules of highly correlated metabolites were identified using the "blockwiseModules" function with the following parameters: minimum module size = 30, merge cut height = 0.25, and deepSplit = 2. Module-trait associations were evaluated by correlating module eigenmetabolites with pro-inflammatory cytokine levels.

Quantification and statistical analysis

An independent Student's t-test was used to determine statistical significance ($p < 0.05$). Multiple treatment groups were compared using one-way ANOVA followed by Dunnett's or Bonferroni's test for multiple comparisons. The significance of omics data was ascertained with PERMANOVA by Adonis (999 permutations). Differential expression analysis by DESeq2 was conducted using the Wilcoxon Test. One-sample t-test was performed to determine the statistical significance of oxidized lipid production. Significance levels were annotated as follows: *, $p < 0.05$; **, $p < 0.01$; ***, $p < 0.001$. Statistical computations and graphical representations were performed in R. Experimental sample sizes and the specific statistical tests are detailed in the figure legends.

Reporting summary

Further information on research design is available in the Nature Portfolio Reporting Summary linked to this article.

Data availability

The RNA-seq data in this study have been deposited in the Genome Sequence Archive (GSA) under accession code subCRA022787 (https://bigd.big.ac.cn/gsa/browse/CRA014284). The metabolomics and lipidomics data generated in this study have been deposited in the Open Archive for Miscellaneous Data (OMIX) under accession code OMIX005531. The Olink proteomics data generated in this study have been deposited in OMIX under accession code OMIX005706. Source data are provided with this paper.

Code availability

The code for all analyzes is available at https://gitee.com/neokie/code-for-nc.

References

1. Armet, A. M. et al. Rethinking healthy eating in light of the gut microbiome. *Cell Host Microbe* **30**, 764–785 (2022).
2. Singh, G. K. & DiBari, J. N. Marked disparities in pre-pregnancy obesity and overweight prevalence among US women by race/ethnicity, nativity/immigrant status, and sociodemographic characteristics, 2012-2014. *J. Obes.* **2019**, 2419263 (2019).

3. Bruce, C. R. & Febbraio, M. A. It's what you do with the fat that matters! *Nat. Med.* **13**, 1137–1138 (2007).
4. Liu, X. et al. High-fiber diet mitigates maternal obesity-induced cognitive and social dysfunction in the offspring via gut-brain axis. *Cell Metab.* **33**, 923–938.e926 (2021).
5. Sgritta, M. et al. Mechanisms underlying microbial-mediated changes in social behavior in mouse models of autism spectrum disorder. *Neuron* **101**, 246–259.e246 (2019).
6. Loomes, R., Hull, L. & Mandy, W. P. L. What is the male-to-female ratio in autism spectrum disorder? a systematic review and meta-analysis. *J. Am. Acad. Child Adolesc. Psychiatry* **56**, 466–474 (2017).
7. Barker-Haliski, M. & Steve White, H. Validated animal models for antiseizure drug (ASD) discovery: advantages and potential pitfalls in ASD screening. *Neuropharmacology* **167**, 107750 (2020).
8. Garidou, L. et al. The gut microbiota regulates intestinal CD4 T cells expressing RORγt and controls metabolic disease. *Cell Metab.* **22**, 100–112 (2015).
9. Shankar, K. Reversing fetal undernutrition by kick-starting early growth. *Endocrinology* **156**, 3059–3062 (2015).
10. Payolla, T. B. et al. High-fat diet during pregnancy and lactation impairs the cholinergic anti-inflammatory pathway in the liver and white adipose tissue of mouse offspring. *Mol. Cell. Endocrinol.* **422**, 192–202 (2016).
11. Hauguel-de Mouzon, S. & Guerre-Millo, M. The placenta cytokine network and inflammatory signals. *Placenta* **27**, 794–798 (2006).
12. Han, V. X., Patel, S., Jones, H. F. & Dale, R. C. Maternal immune activation and neuroinflammation in human neurodevelopmental disorders. *Nat. Rev. Neurol.* **17**, 564–579 (2021).
13. Choi, G. B. et al. The maternal interleukin-17a pathway in mice promotes autism-like phenotypes in offspring. *Sci. (N. Y., NY)* **351**, 933–939 (2016).
14. Lammert, C. R. et al. Cutting Edge: Critical Roles for Microbiota-Mediated Regulation of the Immune System in a Prenatal Immune Activation Model of Autism. *J. Immunol. (Baltim., Md: 1950)* **201**, 845–850 (2018).
15. Shin Yim, Y. et al. Reversing behavioural abnormalities in mice exposed to maternal inflammation. *Nature* **549**, 482–487 (2017).
16. Kalish, B. T. et al. Maternal immune activation in mice disrupts proteostasis in the fetal brain. *Nat. Neurosci.* **24**, 204–213 (2021).
17. McCarthy, M. M. & Wright, C. L. Convergence of sex differences and the neuroimmune system in autism spectrum disorder. *Biol. psychiatry* **81**, 402–410 (2017).
18. Nathan, C. & Ding, A. Nonresolving inflammation. *Cell* **140**, 871–882 (2010).
19. Zmora, N., Bashiardes, S., Levy, M. & Elinav, E. The role of the immune system in metabolic health and disease. *Cell Metab.* **25**, 506–521 (2017).
20. Chan, K. L., Cathomas, F. & Russo, S. J. Central and peripheral inflammation link metabolic syndrome and major depressive disorder. *Physiol. (Bethesda, Md)* **34**, 123–133 (2019).
21. Sun, P. et al. High-fat diet-disturbed gut microbiota-colonocyte interactions contribute to dysregulating peripheral tryptophan-kynurenine metabolism. *Microbiome* **11**, 154 (2023).
22. Ma, N., He, T., Johnston, L. J. & Ma, X. Host-microbiome interactions: the aryl hydrocarbon receptor as a critical node in tryptophan metabolites to brain signaling. *Gut Microbes* **11**, 1203–1219 (2020).
23. Mangge, H. et al. Obesity-related dysregulation of the tryptophan-kynurenine metabolism: role of age and parameters of the metabolic syndrome. *Obes. (Silver Spring, Md)* **22**, 195–201 (2014).
24. Serafini, G. et al. Abnormalities in kynurenine pathway metabolism in treatment-resistant depression and suicidality: a systematic review. *CNS Neurological Disord. drug targets* **16**, 440–453 (2017).
25. Ye, L. et al. IL-1β and TNF-α induce neurotoxicity through glutamate production: a potential role for neuronal glutaminase. *J. Neurochemistry* **125**, 897–908 (2013).
26. Kang, S. S., Kurti, A., Fair, D. A. & Fryer, J. D. Dietary intervention rescues maternal obesity induced behavior deficits and neuroinflammation in offspring. *J. Neuroinflammation* **11**, 156 (2014).
27. Kim, S. et al. Maternal gut bacteria promote neurodevelopmental abnormalities in mouse offspring. *Nature* **549**, 528–532 (2017).
28. Adam, S. et al. Review: Fetal-maternal communication via extracellular vesicles - Implications for complications of pregnancies. *Placenta* **54**, 83–88 (2017).
29. Estes, M. L. & McAllister, A. K. Maternal immune activation: implications for neuropsychiatric disorders. *Sci. (N. Y., NY)* **353**, 772–777 (2016).
30. McAleer, J. P. & Kolls, J. K. Directing traffic: IL-17 and IL-22 coordinate pulmonary immune defense. *Immunological Rev.* **260**, 129–144 (2014).
31. Sun, P. et al. Eucommiae cortex polysaccharides mitigate obesogenic diet-induced cognitive and social dysfunction via modulation of gut microbiota and tryptophan metabolism. *Theranostics* **12**, 3637–3655 (2022).
32. Medina-Rodriguez, E. M., Rice, K. C., Beurel, E. & Jope, R. S. +)-Naloxone blocks Toll-like receptor 4 to ameliorate deleterious effects of stress on male mouse behaviors. *Brain, Behav., Immun.* **90**, 226–234 (2020).
33. Meyer, U. Neurodevelopmental Resilience and Susceptibility to Maternal Immune Activation. *Trends Neurosci.* **42**, 793–806 (2019).
34. Mullins C. A., et al. Neural underpinnings of obesity: the role of oxidative stress and inflammation in the brain. *Antioxidants (Basel, Switzerland)* **9**, 1018 (2020).
35. Canales C. P., et al. Sequential perturbations to mouse corticogenesis following in utero maternal immune activation. *eLife* **10**, e60100 (2021).
36. Cervenka I., Agudelo L. Z., Ruas J. L. Kynurenines: tryptophan's metabolites in exercise, inflammation, and mental health. *Science (New York, NY)* **357**, eaaf9794 (2017).
37. Schwarz, M. J., Guillemin, G. J., Teipel, S. J., Buerger, K. & Hampel, H. Increased 3-hydroxykynurenine serum concentrations differentiate Alzheimer's disease patients from controls. *Eur. Arch. psychiatry Clin. Neurosci.* **263**, 345–352 (2013).
38. Heyes, M. P. et al. Human microglia convert l-tryptophan into the neurotoxin quinolinic acid. *Biochemical J.* **320**, 595–597 (1996).
39. Qin, L. et al. Interactive role of the toll-like receptor 4 and reactive oxygen species in LPS-induced microglia activation. *Glia* **52**, 78–84 (2005).
40. Streit, W. J. Microglial senescence: does the brain's immune system have an expiration date? *Trends Neurosci.* **29**, 506–510 (2006).
41. Chen, Y. et al. Kynurenine-3-monooxygenase (KMO): From its biological functions to therapeutic effect in diseases progression. *J. Cell. Physiol.* **237**, 4339–4355 (2022).
42. Tanaka M., et al. Immune influencers in action: metabolites and enzymes of the tryptophan-kynurenine metabolic pathway. *Biomedicines* **9**, 734 (2021).
43. Miranda, A. F., Boegman, R. J., Beninger, R. J. & Jhamandas, K. Protection against quinolinic acid-mediated excitotoxicity in nigrostriatal dopaminergic neurons by endogenous kynurenic acid. *Neuroscience* **78**, 967–975 (1997).
44. Choi S. C., et al. Gut microbiota dysbiosis and altered tryptophan catabolism contribute to autoimmunity in lupus-susceptible mice. *Sci. Transl. Med.* **12**, eaax2220 (2020).
45. Montgomery, T. L. et al. Lactobacillus reuteri tryptophan metabolism promotes host susceptibility to CNS autoimmunity. *Microbiome* **10**, 198 (2022).

46. Kumar, L. M EF. Mfuzz: a software package for soft clustering of microarray data. *Bioinformation* **2**, 5–7 (2007).
47. Stoner, R. et al. Patches of disorganization in the neocortex of children with autism. *N. Engl. J. Med.* **370**, 1209–1219 (2014).
48. Shi, Y., Kirwan, P., Smith, J., Robinson, H. P. & Livesey, F. J. Human cerebral cortex development from pluripotent stem cells to functional excitatory synapses. *Nat. Neurosci.* **15**, 477–486, s471 (2012).
49. Marín-Padilla, M. Cajal-Retzius cells and the development of the neocortex. *Trends Neurosci.* **21**, 64–71 (1998).
50. Zádori, D., Veres, G., Szalárdy, L., Klivényi, P. & Vécsei, L. Alzheimer's disease: recent concepts on the relation of mitochondrial disturbances, excitotoxicity, neuroinflammation, and kynurenines. *J. Alzheimer's. Dis.: JAD* **62**, 523–547 (2018).
51. Szalardy, L. et al. Mitochondrial disturbances, tryptophan metabolites and neurodegeneration: medicinal chemistry aspects. *Curr. medicinal Chem.* **19**, 1899–1920 (2012).
52. Wu, G., Fang, Y. Z., Yang, S., Lupton, J. R. & Turner, N. D. Glutathione metabolism and its implications for health. *J. Nutr.* **134**, 489–492 (2004).
53. Hou, Y. et al. Mitochondrial superoxide production negatively regulates neural progenitor proliferation and cerebral cortical development. *Stem cells (Dayt., Ohio)* **30**, 2535–2547 (2012).
54. Farooqui, A. A. & Horrocks, L. A. Lipid peroxides in the free radical pathophysiology of brain diseases. *Cell. Mol. Neurobiol.* **18**, 599–608 (1998).
55. Pei, Y. et al. Biological activities and potential oral applications of N-acetylcysteine: progress and prospects. *Oxid. Med. Cell. Longev.* **2018**, 2835787 (2018).
56. Cheroni, C., Caporale, N. & Testa, G. Autism spectrum disorder at the crossroad between genes and environment: contributions, convergences, and interactions in ASD developmental pathophysiology. *Mol. autism* **11**, 69 (2020).
57. Godfrey, K. M. et al. Influence of maternal obesity on the long-term health of offspring. *lancet Diab Endocrinol.* **5**, 53–64 (2017).
58. Saito, T. & Shimazaki, Y. Metabolic disorders related to obesity and periodontal disease. *Periodontology 2000* **43**, 254–266 (2007).
59. Venter C., Eyerich S., Sarin T., Klatt K. C. Nutrition and the immune system: a complicated tango. *Nutrients* **12**, 818 (2020).
60. Yi, Y. S. Regulatory roles of flavonoids on inflammasome activation during inflammatory responses. *Mol. Nutr. food Res.* **62**, e1800147 (2018).
61. Cronkite, D. A. & Strutt, T. M. The regulation of inflammation by innate and adaptive lymphocytes. *J. Immunol. Res.* **2018**, 1467538 (2018).
62. Cai, Z., Pan, Z. L., Pang, Y., Evans, O. B. & Rhodes, P. G. Cytokine induction in fetal rat brains and brain injury in neonatal rats after maternal lipopolysaccharide administration. *Pediatr. Res.* **47**, 64–72 (2000).
63. Wong, H. & Hoeffer, C. Maternal IL-17A in autism. *Exp. Neurol.* **299**, 228–240 (2018).
64. Waisman, A., Hauptmann, J. & Regen, T. The role of IL-17 in CNS diseases. *Acta Neuropathologica* **129**, 625–637 (2015).
65. Norlander A. E., et al. A salt-sensing kinase in T lymphocytes, SGK1, drives hypertension and hypertensive end-organ damage. *JCI insight* **2**, e92801 (2017).
66. Alves de Lima, K. et al. Meningeal γδ T cells regulate anxiety-like behavior via IL-17a signaling in neurons. *Nat. Immunol.* **21**, 1421–1429 (2020).
67. Oren, R., Farnham, A. E., Saito, K., Milofsky, E. & Karnovsky, M. L. Metabolic patterns in three types of phagocytizing cells. *J. Cell Biol.* **17**, 487–501 (1963).
68. O'Neill, L. A., Kishton, R. J. & Rathmell, J. A guide to immunometabolism for immunologists. *Nat. Rev. Immunol.* **16**, 553–565 (2016).
69. Xiao, N. et al. Integrated cytokine and metabolite analysis reveals immunometabolic reprogramming in COVID-19 patients with therapeutic implications. *Nat. Commun.* **12**, 1618 (2021).
70. Romani, L., Zelante, T., De Luca, A., Fallarino, F. & Puccetti, P. IL-17 and therapeutic kynurenines in pathogenic inflammation to fungi. *J. Immunol. (Baltim., Md: 1950)* **180**, 5157–5162 (2008).
71. Huang, Y. S., Ogbechi, J., Clanchy, F. I., Williams, R. O. & Stone, T. W. IDO and Kynurenine Metabolites in Peripheral and CNS Disorders. *Front. Immunol.* **11**, 388 (2020).
72. Wirleitner, B. et al. Immune activation and degradation of tryptophan in coronary heart disease. *Eur. J. Clin. Investig.* **33**, 550–554 (2003).
73. Kwidzinski, E. & Bechmann, I. IDO expression in the brain: a double-edged sword. *J. Mol. Med. (Berl., Ger.)* **85**, 1351–1359 (2007).
74. Speciale, C. & Schwarcz, R. Uptake of kynurenine into rat brain slices. *J. Neurochemistry* **54**, 156–163 (1990).
75. Vécsei, L., Szalárdy, L., Fülöp, F. & Toldi, J. Kynurenines in the CNS: recent advances and new questions. *Nat. Rev. Drug Discov.* **12**, 64–82 (2013).
76. Zengeler, K. E. & Lukens, J. R. Innate immunity at the crossroads of healthy brain maturation and neurodevelopmental disorders. *Nat. Rev. Immunol.* **21**, 454–468 (2021).
77. Hanamsagar, R. et al. Generation of a microglial developmental index in mice and in humans reveals a sex difference in maturation and immune reactivity. *Glia* **65**, 1504–1520 (2017).
78. Markram, H. et al. Interneurons of the neocortical inhibitory system. *Nat. Rev. Neurosci.* **5**, 793–807 (2004).
79. Solecki, D. J. Sticky situations: recent advances in control of cell adhesion during neuronal migration. *Curr. Opin. Neurobiol.* **22**, 791–798 (2012).
80. Crino, P. B., Trojanowski, J. Q. & Eberwine, J. Internexin, MAP1B, and nestin in cortical dysplasia as markers of developmental maturity. *Acta neuropathologica* **93**, 619–627 (1997).
81. Varghese, M. et al. Autism spectrum disorder: neuropathology and animal models. *Acta Neuropathologica* **134**, 537–566 (2017).
82. Knuesel, I. et al. Maternal immune activation and abnormal brain development across CNS disorders. *Nat. Rev. Neurol.* **10**, 643–660 (2014).
83. Whittle, S., Finn, M., Little, K. & Olsson, C. A. A methodological review of fetal neurosonographic studies: New directions in assessment of neurodevelopmental risk for mental health problems. *Neurosci. Biobehav. Rev.* **114**, 172–193 (2020).
84. Garbett, K. A., Hsiao, E. Y., Kálmán, S., Patterson, P. H. & Mirnics, K. Effects of maternal immune activation on gene expression patterns in the fetal brain. *Transl. psychiatry* **2**, e98 (2012).
85. Usui N., Kobayashi H., Shimada S. Neuroinflammation and oxidative stress in the pathogenesis of autism spectrum disorder. *International journal of molecular sciences* **24**, 818 (2023).
86. Bjørklund, G. et al. The role of glutathione redox imbalance in autism spectrum disorder: a review. *Free Radic. Biol. Med.* **160**, 149–162 (2020).
87. Nadarajah, B. & Parnavelas, J. G. Modes of neuronal migration in the developing cerebral cortex. *Nat. Rev. Neurosci.* **3**, 423–432 (2002).
88. Goldstein, J. M. et al. Prenatal maternal immune disruption and sex-dependent risk for psychoses. *Psychological Med.* **44**, 3249–3261 (2014).
89. Gilman, S. E. et al. Prenatal immune programming of the sex-dependent risk for major depression. *Transl. psychiatry* **6**, e822 (2016).
90. Mac Giollabhui, N. et al. Maternal inflammation during pregnancy and offspring psychiatric symptoms in childhood: Timing and sex matter. *J. Psychiatr. Res.* **111**, 96–103 (2019).

91. Jiménez, J. A. & Zylka, M. J. Controlling litter effects to enhance rigor and reproducibility with rodent models of neurodevelopmental disorders. *J. neurodevelopmental Disord.* **13**, 2 (2021).
92. Cabungcal, J. H., Steullet, P., Kraftsik, R., Cuenod, M. & Do, K. Q. Early-life insults impair parvalbumin interneurons via oxidative stress: reversal by N-acetylcysteine. *Biol. psychiatry* **73**, 574–582 (2013).
93. Lai, Y. et al. High-coverage metabolomics uncovers microbiota-driven biochemical landscape of interorgan transport and gut-brain communication in mice. *Nat. Commun.* **12**, 6000 (2021).
94. Shen, X. et al. TidyMass an object-oriented reproducible analysis framework for LC-MS data. *Nat. Commun.* **13**, 4365 (2022).
95. Wishart, D. S. et al. HMDB 5.0: the Human Metabolome Database for 2022. *Nucleic Acids Res* **50**, D622–d631 (2022).
96. Chong, J., Wishart, D. S. & Xia, J. Using metaboanalyst 4.0 for comprehensive and integrative metabolomics data analysis. *Curr. Protoc. Bioinforma.* **68**, e86 (2019).
97. Bolger, A. M., Lohse, M. & Usadel, B. Trimmomatic: a flexible trimmer for Illumina sequence data. *Bioinformatics* **30**, 2114–2120 (2014).
98. Liao, Y., Smyth, G. K. & Shi, W. featureCounts: an efficient general purpose program for assigning sequence reads to genomic features. *Bioinformatics* **30**, 923–930 (2014).
99. Barupal, D. K. & Fiehn, O. Chemical similarity enrichment analysis (ChemRICH) as alternative to biochemical pathway mapping for metabolomic datasets. *Sci. Rep.* **7**, 14567 (2017).
100. Love, M. I., Huber, W. & Anders, S. Moderated estimation of fold change and dispersion for RNA-seq data with DESeq2. *Genome Biol.* **15**, 550 (2014).
101. Zhou, Y. et al. Metascape provides a biologist-oriented resource for the analysis of systems-level datasets. *Nat. Commun.* **10**, 1523 (2019).
102. Wu, T. et al. clusterProfiler 4.0: A universal enrichment tool for interpreting omics data. *Innov. (Camb. (Mass))* **2**, 100141 (2021).
103. Lazic, S. E. & Essioux, L. Improving basic and translational science by accounting for litter-to-litter variation in animal models. *BMC Neurosci.* **14**, 37 (2013).

Acknowledgements

The study was financially supported by Foundation for top talent recruitment of Xi'an Medical College (No. 2018RCYJ04, X.J.C), Key Research & Development projects of Shaanxi Province (No.2020QFY10-04, S.T.Z and X.J.C), "Tianfu Scholar" distinguished expert program of Sichuan Province (No. 2020-120, S.T.Z) and 17th Eucommia Research Grant from Eucommia ulmoides Research Association of Japan (No. 2022, X.J.C), and Agricultural Science and Technology Innovation Program (No.CAAS-ZDRW202308, Y.X.L). In this study, confocal microscope image acquisition was facilitated by the Technological Innovation and Talent Cultivation Platform of Northwest A&F University.

Author contributions

P.H.S. and M.L.W. contributed equally to this work. Conceptualization S.T.Z., P.H.S., and M.L.W.; methodology: S.T.Z., P.H.S., M.L.W., Y.X.L., W.Z., and L.Q.L.; investigation P.H.S, M.L.W., S.T.Z., X.J.C., X.Y.Z., S.L.C., and L.Q.L.; formal analysis P.H.S., M.L.W., Y.X.L., L.Q.L., and W.Z.; writing-original draft P.H.S. and M.L.W.; writing-review & editing S.T.Z., X.Y.Z., S.L.C., and X.J.C.; visualization P.H.S. and M.L.W.; supervision S.T.Z.; project administration S.T.Z.; funding acquisition S.T.Z., X.J.C., and Y.X.L.

Competing interests

The authors declare that they have no competing interests.

Additional information

Supplementary information The online version contains supplementary material available at https://doi.org/10.1038/s41467-025-57414-4.

Correspondence and requests for materials should be addressed to Xuejun Chai, Xiaoyan Zhu or Shanting Zhao.

Peer review information *Nature Communications* thanks the anonymous reviewers for their contribution to the peer review of this work. A peer review file is available.